J. Fluid Mech. (2002), *vol.* 464, *pp.* 35–80.
DOI: 10.1017/S0022112002008753 Printed in the United Kingdom

Extension of second-order Stokes theory to variable bathymetry

By K. A. BELIBASSAKIS AND G. A. ATHANASSOULIS

Department of Naval Architecture and Marine Engineering, National Technical University of Athens, PO Box 64033 Zografos, 15710 Athens, Greece
kbel@fluid.mech.ntua.gr; mathan@central.ntua.gr

(Received 25 October 2000 and in revised form 28 January 2002)

In the present work second-order Stokes theory has been extended to the case of a generally shaped bottom profile connecting two half-strips of constant (but possibly different) depths, initiating a method for generalizing the Stokes hierarchy of second- and higher-order wave theory, without the assumption of spatial periodicity. In modelling the wave–bottom interaction three partial problems arise: the first order, the unsteady second order and the steady second order. The three problems are solved by using appropriate extensions of the consistent coupled-mode theory developed by the present authors for the linearized problem. Apart from the Stokes small-amplitude expansibility assumption, no additional asymptotic assumptions have been introduced. Thus, bottom slope and curvature may be arbitrary, provided that the resulting wave dynamics is Stokes-compatible. Accordingly, the present theory can be used for the study of various wave phenomena (propagation, reflection, diffraction) arising from the interaction of weakly nonlinear waves with a general bottom topography, in intermediate water depth. An interesting phenomenon, that is also very naturally resolved, is the net mass flux induced by the depth variation, which is consistently calculated by means of the steady second-order potential. The present method has been validated against experimental results and fully nonlinear numerical solutions. It has been found that it correctly predicts the second-order harmonic generation, the amplitude nonlinearity, and the amplitude variation due to non-resonant first-and-second harmonic interaction, up to the point where the energy transfer to the third and higher harmonics can no longer be neglected. Under the restriction of weak nonlinearity, the present model can be extended to treat obliquely incident waves and the resulting second-order refraction patterns, and to study bichromatic and/or bidirectional wave–wave interactions, with application to the transformation of second-order random seas in variable bathymetry regions.

1. Introduction

We consider the problem of weakly nonlinear gravity waves normally incident on a smooth, but possibly steep, two-dimensional shoal; see figure 1. An essential feature of this problem is that the wave field is not spatially periodic. Extra difficulties are introduced by the fact that we drop the assumptions of smallness of the bottom slope and curvature.

An important phenomenon that can be analysed by means of a weakly nonlinear theory, appropriately adjusted to the variable bathymetry case, is the phenomenon of harmonic generation due to nonlinear wave–bottom interaction. This phenomenon

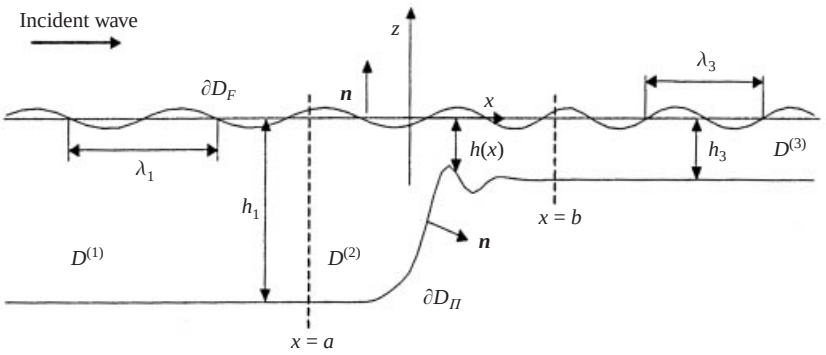

FIGURE 1. Geometrical configuration and basic notation.

has been observed in waves propagating from deep water to the continental shelf (see e.g. the description in the introductions of Massel 1983 and Grue 1992), and in the laboratory, in the case of waves propagating over submerged structures (Bendykowska & Massel 1984; Grue 1992; Rey, Belzons & Guazzelli 1992; Beji & Battjes 1993; Losada, Patterson & Losada 1997). It strongly affects the wave spectrum transformation over variable bathymetry regions (Kojima, Kioka & Yoshida 1990; Ohyama & Nadaoka 1994), and is important for the prediction of wave properties in the coastal and surf zone. Another phenomenon that can be resolved by a weakly nonlinear theory is the recurring evolution of water waves, appearing as a result of non-resonant interactions between the various wave harmonics. This phenomenon was observed (as a nuisance) many years ago in laboratory experiments, and studied by various authors, e.g. Fontanet (1961), Hulsbergen (1974), Massel (1983), Bendykowska & Massel (1988), Goda (1997). In the last paper an historical survey is also presented.

The interaction of free-surface gravity waves with uneven bottom topography requires, in principle, the solution of a complicated nonlinear boundary value problem. Although viscous free-surface flow simulations over variable bottom topographies are nowadays possible, they are extremely demanding computationally. Recent studies concentrate on the effects of flow separation and vortex generation, such as in the case of waves propagating over a submerged dike (Huang & Dong 1999). In general, however, the problem is treated in the framework of potential flow (Tsai & Yue 1996). Even under this assumption, the complete numerical solution to the nonlinear free-surface problem presents great difficulties. Time-domain numerical methods for treating the fully nonlinear problem have been developed by Longuet-Higgins & Cokelet (1976) and Vinje & Brevig (1981), and since then they have been used by many authors, see e.g. Isaacson (1982), Dommermuth & Yue (1987), Ohyama & Nadaoka (1991, 1994) and the survey by Tsai & Yue (1996). The main difficulty in this approach is the excessive computational effort required, especially in connection with coastal applications where the range of propagation is usually large. In order to improve efficiency, Wang, Mirie & Tulin (1995) proposed a multi-subdomain approach and Kennedy & Fenton (1999) introduced the local polynomial approximation, satisfying the Laplace equation within each subdomain. Still, however, considerable computer requirements limit the use of the above fully nonlinear models in practical applications.

On the other hand, there is a vast literature on simplified model wave equations, mainly based on the assumptions of weak free-surface nonlinearity and slowly varying bathymetry. These model equations have a more conventional form, permitting the development of relevant theoretical results, and they are more efficient computa-

tionally, within the range of their applicability. For example, combining appropriate asymptotic treatment with depth integration, a class of *Boussinesq-type* models is derived, accounting for the effects of weak nonlinearity and dispersion for shallow water waves. Improved versions of these models with enhanced dispersion characteristics, extending the range of applicability to larger depths and/or variable bathymetry, have been reported by many authors, see e.g. Madsen & Sorensen (1992), Nwogu (1993), Liu (1995), Kirby (1997), and the references cited therein. In general, however, these models cannot be relied on as the depth increases, or the bathymetry is not slowly varying. Another important example is a class of models that can be considered as weakly nonlinear generalizations of the *mild-slope* equation, e.g. the models developed by Beji & Nadaoka (1997), Nadaoka, Beji & Nakagawa (1997), Tang & Ouellet (1997). These models can describe combined refraction–diffraction of weakly nonlinear water waves, but still suffer from the assumption of slowly varying bathymetries.

In the case of not very shallow water, another typical approach is to use *Stokes-type* asymptotic expansions of the velocity potential and free-surface elevation, using as perturbation parameter the wave slope or an equivalent quantity, see e.g. Mei (1989), Dingemans (1997, § 2.8). This approach has been comprehensively developed for the case of constant depth. For example, through a series of papers (see e.g. Fenton 1985; Jonsson & Arneborg 1995 and the references cited therein) a complete theory has been developed up to the fifth-order for unidirectional waves, while Ohyama, Jeng & Hsu (1995*a*) have developed a fourth-order theory for multidirectional waves. In the present work the Stokes approach is extended to the case of a generally shaped bottom profile connecting two half-strips of constant but (possibly) different depths, initiating a method for generalizing the Stokes hierarchy of wave theories to the variable bathymetry case, i.e. without the assumption of spatial periodicity.

The second-order Stokes theory for waves lacking spatial periodicity (necessitating, thus, the inclusion of evanescent modes) has been already used for analysing a number of problems, both in the frequency and in the time domains. For example, Hudspeth & Sulisz (1991), Moubayed & Williams (1994) and Schaeffer (1996) have developed second-order wavemaker theories, and there has been much work on second-order wave–body interactions in the case of a scatterer in a constant-depth strip; some recent references are Sulitz (1993, 1999), Drimer & Agnon (1994), Newman (1996), Huang & Eatock Taylor (1996), Li & Williams (1998), Teng & Kato (1999), Malenica, Eatock Taylor & Huang (1999). For the calculation of second-order forces and moments on bodies, an indirect method, without necessitating the calculation of the second-order potential, has been suggested by Lighthill (1979) for infinite water depth, extended to the case of a vertical cylinder in finite water depth by Molin (1979), and since then used by many authors. The second-order diffraction problem has also been treated in the time domain by Isaacson & Cheung (1991, 1992). The characteristic feature of all the above work is that the water depth is considered constant throughout the liquid domain. A case of non-constant depth has been considered by Massel (1983) and Bendykowska & Massel (1984), who have studied both theoretically and experimentally the second-order propagation–diffraction problem for a monochromatic wave normally incident on an infinite underwater step. More recently Rhee (1997) considered this problem for an obliquely incident wave.

Our main concern here is to develop a second-order Stokes theory for the case of a smooth, generally shaped bathymetry, without imposing any mild-slope-type assumptions on the bottom boundary. (This means that the bathymetry may change

considerably within one wavelength distance.) Clearly, the second-order solution has to be based on a reliable first-order one, conforming to the same specifications. For this purpose, the *consistent coupled-mode theory* developed by Athanassoulis & Belibassakis (1999, referred to herein as AB) is used. This method transforms the linearized problem to a coupled system of horizontal second-order differential equations, and can be considered as an improvement of the extended mild-slope equation developed by Massel (1993) and Porter & Staziker (1995). It applies domain decomposition to three subdomains: two infinite half-strips of constant (possibly different) depths, and a bounded, variable bathymetry subdomain between the two half-strips. Wave potential is represented by means of complete normal-mode series in the two half-strips, and by an enhanced *local-mode* series in the intermediate, variable bathymetry subdomain. The latter series involves the propagating and evanescent modes and, also, an additional term, called the *sloping-bottom mode*, which allows the exact satisfaction of the bottom boundary condition, even on the steep parts of the bottom. This method has also been extended to three dimensions (Athanassoulis, Belibassakis & Gerostathis 2000).

To obtain the solution to the second-order problem, an incident wave system should be defined, and appropriate conditions, controlling the behaviour of the second-order potentials at infinity, must be introduced. In formulating the monochromatic second-order diffraction problem, the incident wave field is usually taken to be the superposition of the first harmonic and the associated Stokes second-order bound wave, see e.g. Molin (1979) and the references cited above in connection with the wave–body interaction problem. The same definition of the incident wave has also been made by Massel (1983) and Rhee (1997) in the case of an infinite underwater step. In the present work the incident wave system is generalized by including a double-frequency free harmonic, with an arbitrary second-order amplitude. Such a component might, in fact, be present if the incident wave system is generated by the wavemaker in a flume (Hudspeth & Sulisz 1991; Goda 1997), or disturbed by another bottom inhomogeneity located far up-wave. (In these cases the amplitude of the incident double-frequency free harmonic can be calculated by taking into account the details of the up-wave flow). Concerning conditions at infinity, the usual radiation condition (Massel 1983; Sulisz 1993), stating that the second-order free waves generated by the bottom inhomogeneity propagate outwards, has been used. It has been implemented in a straightforward way, by retaining only the outward-propagating free-wave modes in the series representations used in the solution procedure.

Unlike the case of waves propagating in uniform depth, in the case of an uneven bottom topography, the average second-order mass flux generated by the first-order wave is not balanced. This inconsistency is resolved by taking into account the steady second-order potential, which behaves like a uniform current at infinity. It is shown here that the total mass flux up to the second order, i.e. that generated by linearized potential plus that induced by the steady second-order problem, is the same across any vertical section.

Thanks to the assumption that far from the bottom inhomogeneity the depth is constant (although it may be different up- and down-wave), the problem can be treated similarly to the linearized one (see AB), i.e. by applying domain decomposition and by requiring the complete matching of the second-order wave potential at the artificial vertical interfaces, separating the infinite half-strips from the bounded, variable bathymetry region. Complete normal-mode representations of the wave potential up to second-order have been used in the two half-strips, and enhanced local-mode representations have been used in the variable bathymetry domain. The

latter representations contain, apart from the standard set of modes (propagating and evanescent), two additional modes: the *free-surface mode*, enabling the exact satisfaction of the inhomogeneous free-surface condition, and the *sloping-bottom mode*, serving the same purpose as in the linearized problem (AB, § 4). The second-order problems are finally refomulated, with the aid of appropriate variational principles, as coupled-mode systems of second-order differential equations in the propagation (horizontal) space, restricted by the bounded extent of the free surface of the intermediate subdomain. Complete sets of boundary conditions for each system of equations are derived with the aid of the variational formulations. The final systems are similar to the corresponding one obtained in AB for the linearized problem, with the appropriate non-homogeneities bringing into play the second-order effects.

Approximate numerical solutions are obtained by truncating the local-mode series to a finite number of terms, and using finite differences for the discretization of the horizontal coupled-mode systems. A thorough numerical investigation has been performed in the case of a smooth underwater shoaling with a very steep bottom, mainly aimed at the determination of appropriate values for the numerical parameters, and the establishment of numerical convergence. One finding is that the rate of decay of the second-order modal-amplitude functions is $O(n^{-4})$, where n is the mode number, as in the linearized problem (AB, § 6). This means that a small number of modes is sufficient to accurately calculate the second-order velocity field throughout the liquid domain, also including the steep parts of the bottom boundary.

The present method has also been validated against experimental results (Rey *et al.* 1992; Ohyama, Kioka & Tada 1995*b*) and fully nonlinear numerical solutions (Ohyama & Nadaoka 1994). It has been found that it correctly predicts the second-order harmonic generation, the amplitude nonlinearity, and the amplitude variation down-wave due to non-resonant first-and-second harmonic interaction, up to a limiting shoaling configuration, after which a large amount of energy is transferred to higher harmonics.

The present work is structured as follows. In § 2 the boundary-value problem is formulated in the time and frequency domains. In § 3 energy and mass fluxes are studied up to the second order. Complete representations for the second-order potentials in the constant-depth half-strips are given in § 4. In § 5 the second-order problems are reformulated as matching boundary-value (transmission) problems, and equivalent variational principles are given. The enhanced local-mode representations in the variable bathymetry domain are derived in § 6. The second-order problems are reformulated as coupled-mode systems of horizontal differential equations in § 7. In § 8 numerical results are presented and discussed, and the conclusions are stated in § 9. Various technical details are included in three appendices.

2. Formulation of the problem

The geometrical configuration for the wave problem under study is shown in figure 1. Geometrical notation and terminology are the same as in our previous paper (AB), to which the reader is referred for detailed definitions. Here we restrict ourselves to mentioning that the whole domain D is a two-dimensional strip, horizontally unbounded, ending in the constant-depth half-strips $D^{(1)}$ (left half-strip, region of incidence, of depth h_1), and $D^{(3)}$ (right half-strip, region of transmission, of depth h_3). The bounded subdomain $D^{(2)}$, joining the two half-strips $D^{(1)}$ and $D^{(3)}$, contains the whole varying-depth region. Anticipating the physical formulation (see below), we state that

the wave propagation–reflection problem in D will be eventually reformulated as a transmission problem within the finite subdomain $D^{(2)}$.

Still-water depth is denoted by $h(x)$, and is a twice continuously differentiable function defined on the real axis $\mathbb{R}$, such that

$$h(x) = h(a) = h_1 \quad \text{for all} \quad x \leqslant a, \quad h(x) = h(b) = h_3 \quad \text{for all} \quad x \geqslant b. \tag{2.1}$$

Thus, $D^{(2)}$ is separated from the two half-strips $D^{(1)}$ and $D^{(3)}$ by means of the vertical interfaces at $x = a$ and $x = b$, respectively, shown as vertical dashed lines in figure 1. Also, $h(x)$ can be considered as the mean water depth at each position x corresponding to linearized waves. Note, however, that in the case of nonlinear waves the mean water depth at each position x does not coincide with $h(x)$. This point will be discussed in more detail below.

2.1. *The incident wave system*

The wave field is generated by the incidence of a second-order periodic wave system of fundamental frequency ω, propagating from $D^{(1)}$ to $D^{(3)}$, with direction normal to the bottom contours. That is, the incident wave system is the complete, second-order Stokes wave system corresponding to the depth h_1, travelling in the positive x-direction. It consists of the linearized incident wave $\Phi^{inc}_{(1)}(x,z;t)$, of frequency ω and height H, and the second-order Stokes component $\Phi^{inc}_{(2b)}(x,z;t)$ bound to the linearized wave. In addition to the above components, a second-order free harmonic $\Phi^{inc}_{(2f)}(x,z;t)$ is also included in the incident wave system; it is assumed to have an arbitrary amplitude consistent, however, with the order of approximation. Thus, the wave potential associated with the incident wave system is as follows:

$$\begin{aligned}\Phi^{inc}(x,z;t) &= \Phi^{inc}_{(1)}(x,z;t) + \Phi^{inc}_{(2b)}(x,z;t) + \Phi^{inc}_{(2f)}(x,z;t)\\ &= -\frac{gH}{2\omega}\frac{\cosh(k_0^{(1)}(z+h_1))}{\cosh(k_0^{(1)}h_1)}\mathrm{Re}(\mathrm{i}A_0\exp(\mathrm{i}(k_0^{(1)}x-\omega t)))\\ &\quad -\frac{3H^2\omega}{32}\frac{\cosh(2k_0^{(1)}(z+h_1))}{\sinh^4(k_0^{(1)}h_1)}\mathrm{Re}(\mathrm{i}A_0^2\exp(2\mathrm{i}(k_0^{(1)}x-\omega t)))\\ &\quad -\frac{H^2\omega}{4}\frac{\cosh(\kappa_0^{(1)}(z+h_1))}{\cosh(\kappa_0^{(1)}h_1)}\mathrm{Re}(\Lambda_0\exp(\mathrm{i}(\kappa_0^{(1)}x-2\omega t))),\end{aligned} \tag{2.2a}$$

where $\mathrm{i} = \sqrt{-1}$; the quantities $k_0^{(1)}$ and $\kappa_0^{(1)}$ are appropriate wavenumbers obtained as the roots of the dispersion relations $\mu h_1 = k_0^{(1)}h_1\tanh(k_0^{(1)}h_1)$ and $4\mu h_1 = \kappa_0^{(1)}h_1\tanh(\kappa_0^{(1)}h_1)$, respectively; $\mu = \omega^2/g$ is the frequency parameter and g is the acceleration due to gravity. Furthermore, $A_0 = \exp(\mathrm{i}\theta_0)$ is an arbitrary constant controlling the phase of the linearized component $\Phi^{inc}_{(1)}(x,z;t)$, and Λ_0 is an arbitrary constant with modulus $|\Lambda_0| = O(1)$ controlling the amplitude and the phase of the second-order free harmonic $\Phi^{inc}_{(2f)}(x,z;t)$. It can be easily seen that the requirement $|\Lambda_0| = O(1)$, in conjunction with the multiplicative constant $H^2\omega/4$, renders the wave slope associated with $\Phi^{inc}_{(2f)}(x,z;t)$ of second-order in comparison with the wave slope of $\Phi^{inc}_{(1)}(x,z;t)$.

For given wave frequency ω and wave height H, the degrees of freedom of the incident system (2.2a) are the complex constants A_0 and Λ_0. The inclusion of the second-order free harmonic $\Phi^{inc}_{(2f)}(x,z;t)$ as an extra, independent component, permits us to formulate and study the complete transmission–diffraction–reflection problem of second-order Stokes waves in a variable bathymetry region, for the most general

forcing by a second-order left-incident wave. This case will be called the *generalized monochromatic* incidence.

The free-surface elevation associated with the incident wave potential (2.2*a*) is given by

$$\eta^{inc}(x;t) = -\frac{H}{8}\frac{1}{\sinh(2k_0^{(1)}h_1)} + \frac{H}{2}\mathrm{Re}(A_0\exp(\mathrm{i}(k_0^{(1)}x - \omega t)))$$
$$+\frac{H^2k_0^{(1)}}{16}\frac{\cosh(k_0^{(1)}h_1)(2+\cosh(2k_0^{(1)}h_1))}{\sinh^3(k_0^{(1)}h_1)}\mathrm{Re}(A_0^2\exp(2\mathrm{i}(k_0^{(1)}x - \omega t)))$$
$$-\frac{H^2\omega^2}{2g}\mathrm{Re}(\mathrm{i}A_0\exp(\mathrm{i}(\kappa_0^{(1)}x - 2\omega t))). \tag{2.2b}$$

The first term in the expansion (2.2*b*) is a constant negative term, which is referred to as the *mean-water-level set-down*, see e.g. Mei (1989, § 12.3), Massel (1989, § 2.3). It is well known (see e.g. Whitham 1974; Dalzell 1999) that in formulating and solving the second-order Stokes problem in constant (finite) water depth, the mean (over a period) wave elevation and the mean wave potential cannot both be zero. In the present approach we shall impose the solution to attain a non-zero mean water elevation and a zero mean wave potential, as anticipated by (2.2) for the incident wave system. With this definition, the energy flux, which will be studied in § 4, should be considered with respect to a mean energy level that coincides with the mean water level of the linearized waves; see also Jonsson & Arneborg (1995).

It is worth noting here that with the incident wave system is associated a mean (over a wave period) mass flux, which, to second order, is given by

$$M_{av}^W = \frac{\rho\omega H^2}{8\tanh(k_0^{(1)}h_1)}. \tag{2.2c}$$

2.2. *Stokes series expansion of the wave potential*

Under the assumption of inviscid and irrotational flow, the wave potential satisfies the following equations in the time domain (see e.g. Mei 1989; chap. 1; Debnath 1994):

$$\Delta\Phi = 0, \quad -\infty < x < \infty, \quad -h(x) < z < \eta(x;t), \tag{2.3a}$$

$$\frac{\partial^2\Phi}{\partial t^2} + g\frac{\partial\Phi}{\partial z} + \frac{\partial|\boldsymbol{u}|^2}{\partial t} + \tfrac{1}{2}\boldsymbol{u}\cdot\nabla|\boldsymbol{u}|^2 = 0, \quad z = \eta(x;t), \tag{2.3b}$$

$$\frac{\partial\Phi}{\partial t} + \tfrac{1}{2}|\boldsymbol{u}|^2 + g\eta = 0, \qquad z = \eta(x;t), \tag{2.3c}$$

$$\frac{\partial\Phi}{\partial z} + \frac{\mathrm{d}h}{\mathrm{d}x}\frac{\partial\Phi}{\partial x} = 0, \qquad z = -h(x), \tag{2.3d}$$

where $\boldsymbol{u} = \nabla\Phi$ is the wave velocity and $\eta(x;t)$ is the free-surface elevation. The problem is restricted in two space dimensions (x, z), since the direction of the incident wave system has been assumed normal to the parallel bottom contours.

The characteristic time scale involved in the problem is the wave period T, related to the fundamental frequency ω by $T = 2\pi/\omega$. The characteristic length scales involved (directly or indirectly) in the problem are: the two far-field water depths h_i, $i = 1, 3$,

the corresponding far-field wavelengths λ_i, $i = 1, 3$, the amplitude of the fundamental harmonic $H/2$, as well as the bottom variation length and an average amplitude of bottom corrugations. Assuming that the water depth does not become extremely small in D, we can select as characteristic vertical scale the quantity $h_{ref} = \frac{1}{2}(h_1 + h_3)$ and as characteristic horizontal scale the deep-water wavelength $\lambda_{ref} = gT^2/2\pi$.

From these characteristic scales we can form various non-dimensional characteristic numbers, the most important of which are: the *shallowness ratios* h_i/λ_i, $i = 1, 3$, and h_{ref}/λ_{ref}, the *mean* and the *maximum bottom slopes* s_{mean}, s_{max}, the *shoaling ratio* h_3/h_1, as well as the nonlinearity parameter

$$\varepsilon = \mu\frac{H}{2} = \frac{\omega^2 H}{2g} = \frac{\pi H}{\lambda_{ref}}. \tag{2.4}$$

Note that, in accordance with the above definition, the nonlinearity parameter ε remains constant in the whole domain $D = D^{(1)} \cup D^{(2)} \cup D^{(3)}$. Since, however, ε coincides with the deep-water wave slope amplitude, the validity of the above non-dimensionalization is, in principle, restricted to the large and intermediate water depth regime (e.g. $h/\lambda \geqslant 0.07$).

In the present work all the above non-dimensional numbers, except the nonlinearity parameter ε, are considered to be of the same order of magnitude, $O(1)$. That is, no asymptotic assumptions are made for them. On the other hand, the nonlinearity parameter ε is assumed to be small, permitting a Stokes-type perturbation expansion to be applied of the form

$$\Phi(x, z, t; \varepsilon) = \varepsilon\phi_1(x, z; t) + \varepsilon^2\phi_2(x, z; t) + \cdots, \tag{2.5}$$

$$\eta(x, t; \varepsilon) = \varepsilon\eta_1(x; t) + \varepsilon^2\eta_2(x; t) + \cdots. \tag{2.6}$$

By introducing the expansions (2.5) and (2.6) in (2.3), and keeping terms up to the second order $O(\varepsilon^2)$, we obtain the linearized and the second-order problems for the pairs $(\phi_1(x, z; t), \eta_1(x; t))$ and $(\phi_2(x, z; t), \eta_2(x; t))$, respectively; see e.g. Mei (1989), Debnath (1994). Conditions at infinity will be discussed in § 2.4, for the time-harmonic case.

2.3. *Harmonic time dependence*

The harmonic time-dependence of the linearized wave potential is introduced by the usual factorization:

$$\phi_1(x, z; t) = \mathrm{Re}(\Xi\varphi_1(x, z; \mu)\mathrm{e}^{-\mathrm{i}\omega t}), \tag{2.7a}$$

where $\Xi = -\mathrm{i}g^2/\omega^3$ is a multiplicative constant, permitting us to write the linearized free-surface elevation (the first term of the Stokes series, (2.6)) in the standard form

$$\varepsilon\eta_1(x, z; t) = \mathrm{Re}(\tfrac{1}{2}H\varphi_1(x, z = 0; \mu)\mathrm{e}^{-\mathrm{i}\omega t}). \tag{2.7b}$$

Using (2.7a) in the free-surface boundary condition of the second-order problem, we see that the forcing term contains the $\omega + \omega = 2\omega$ and $\omega - \omega = 0$ harmonics, as expected. Therefore, the time dependence of the second-order potential should be of the form

$$\phi_2(x, z; t) = \mathrm{Re}(\Xi^2\varphi_{20}(x, z)) + \mathrm{Re}(\Xi^2\varphi_{22}(x, z; \mu_2)\mathrm{e}^{-2\mathrm{i}\omega t}), \tag{2.8a}$$

where $\mu_2 = (2\omega)^2/g = 4\mu$ is the second-order frequency parameter. Thus, the second-order term in the Stokes series expansion of the free-surface elevation, (2.6),

becomes

$$\varepsilon^2\eta_2(x;t) = \varepsilon^2(\eta_{20}(x) + \mathrm{Re}(\eta_{22}(x)\mathrm{e}^{-2\mathrm{i}\omega t})) \\ = (\varepsilon\Xi)^2\left\{\frac{G_{20}}{g} + \mathrm{Re}\left(\left(\frac{2\mathrm{i}\omega}{g}\varphi_{22}(x, z=0) + \frac{G_{22}}{g}\right)\mathrm{e}^{-2\mathrm{i}\omega t}\right)\right\}, \quad (2.8b)$$

where the terms G_{2r}, $r = 0, 2$, are defined exclusively in terms of the linearized potential on the undisturbed free surface, $\varphi_1(x, z = 0)$, as follows:

$$G_{20}(x) = \tfrac{1}{4}|\nabla\varphi_1(x, z=0)|^2 - \tfrac{1}{2}\mu^2|\varphi_1(x, z=0)|^2, \quad (2.8c)$$

$$G_{22}(x) = -\tfrac{1}{4}(\nabla\varphi_1(x, z=0))^2 - \tfrac{1}{2}\mu^2(\varphi_1(x, z=0))^2. \quad (2.8d)$$

2.4. *Conditions at infinity*

Conditions at infinity are suggested by the fundamental physics of the problem under consideration, and they are finely tuned in accordance with the mathematical structure of the analytic model in a way ensuring physical consistency and unique solvability. Since the problem under study is primarily a diffraction problem, the appropriate conditions at infinity are *radiation conditions*, expressing that far from the bottom inhomogeneity the diffracted field behaves like outgoing (reflected in $D^{(1)}$, and transmitted in $D^{(3)}$) waves. Furthermore, since we follow an asymptotic approach, it is natural to introduce radiation conditions separately for the first-order (linearized) and the second-order problems. Following this line of thought, we assume that, far from the inhomogeneity, in the region of incidence ($x \to -\infty$), the wave field up to the second order will contain the following components:

(Ii) the basic first harmonic associated with the incident wave $(\underset{\rightarrow}{\omega}, \lambda_1)$, with given (first-order) amplitude and phase,

(Iii) the reflected first harmonic $(\underset{\leftarrow}{\omega}, \lambda_1)$, with unknown amplitude and phase,

(Iiii) the Stokes second harmonic $(\underset{\rightarrow}{2\omega}, \lambda_{1/2})$ bound up with the basic first harmonic,

(Iiv) the Stokes second harmonic $(\underset{\leftarrow}{2\omega}, \lambda_{1/2})$ bound up with the reflected first harmonic,

(Iv) the incident free second harmonic $(\underset{\rightarrow}{2\omega}, l_1)$, with given (second-order) amplitude and phase, and

(Ivi) the generated free second harmonic $(\underset{\leftarrow}{2\omega}, l_1)$, with unknown amplitude and phase.

In the region of transmission ($x \to \infty$) the wave field up to the second order is assumed to contain the following components:

(Ti) the transmitted first harmonic $(\underset{\rightarrow}{\omega}, \lambda_3)$, with unknown amplitude and phase,

(Tii) the Stokes second harmonic $(\underset{\rightarrow}{2\omega}, \lambda_{3/2})$ bound up with the transmitted first harmonic, and

(Tiii) the generated free second harmonic $(\underset{\rightarrow}{2\omega}, l_3)$, with unknown amplitude and phase.

In the above statements $\lambda_j = 2\pi/k_0^{(j)}$ are the first-order wavelengths in the regions $D^{(j)}$, $j = 1, 3$, obtained by the dispersion relations $\omega^2 = k_0^{(i)} g \tanh(k_0^{(i)} h_i)$; l_i, $i = 1, 3$, are the wavelengths of the free second-harmonic components determined also by the same dispersion relations at the double frequency 2ω. The arrow under the frequency symbol indicates the direction of propagation of the corresponding component.

The above first list of six wave components contains both known forcing terms (to be referred to as 'forcing from infinity') and unknown reflected wave components.

$-\infty < x < +\infty$	*The linearized* (ω) *problem*	*The unsteady* (2ω) *second-order problem*	*The steady second-order problem*
$h < z < 0$	$\Delta\varphi_1 = 0$	$\Delta\varphi_{22} = 0$	$\Delta\varphi_{20} = 0$
$z = 0$	$\dfrac{\partial\varphi_1}{\partial z} - \mu\varphi_1 = 0$	$\dfrac{\partial\varphi_{22}}{\partial z} - \mu_2\varphi_{22} = F_{22}$	$\dfrac{\partial\varphi_{20}}{\partial z} = \tilde{F}_{20}$
$z = -h(x)$	$\dfrac{\partial\varphi_1}{\partial z} + \dfrac{\mathrm{d}h}{\mathrm{d}x}\dfrac{\partial\varphi_1}{\partial x} = 0$	$\dfrac{\partial\varphi_{22}}{\partial z} + \dfrac{\mathrm{d}h}{\mathrm{d}x}\dfrac{\partial\varphi_{22}}{\partial x} = 0$	$\dfrac{\partial\varphi_{20}}{\partial z} + \dfrac{\mathrm{d}h}{\mathrm{d}x}\dfrac{\partial\varphi_{20}}{\partial x} = 0$
Forcing from infinity	(Ii)	(Iiii), (Iiv), (Iv) and (Tii)	not present
Conditions at infinity	(Iii) and (Ti) (radiation condition)	(Ivi) and (Tiii) (radiation condition)	(Ivii) and (Tiv)

TABLE 1. Linearized and second-order problems in the frequency domain.

(Ii) is the usual first-order forcing from infinity; (Iiii), (Iiv) and (Iv) are forcing from infinity for the second-order problem; (Iii) and (Ivi) are the first- and second-order reflected wave components, whose amplitude and phase will be determined through the solution procedure. In the second list, the components (Ti) and (Tiii) are first- and second-order transmitted waves, which will be determined by the solution, while (Tii) constitutes a forcing from infinity of the second-order problem.

Conditions (Iii) and (Ti) constitute the (usual) *radiation conditions of the linearized problem.* Conditions (Ivi) and (Tiii) constitute *the radiation conditions of the* 2ω *problem.* We mention here that all the components listed above, except (Iv), which is considered for the first time herein, have been also used by Massel (1983) in the study of second-order Stokes waves over an abrupt underwater step; see also Massel (1989).

As will be discussed in more detail later in §4, the (second-order) mass fluxes through the constant-depth subdomains $D^{(1)}$ $(x \to -\infty)$ and $D^{(3)}$ $(x \to +\infty)$, as calculated from the linearized potential $\varphi_1(x, z)$, are not equal. This mass unbalance can only be recovered by the steady second-order wave potential $\varphi_{20}(x, z)$. Therefore, it is reasonable to assume that $\varphi_{20}(x, z)$ behaves like a uniform current at infinity, with direction and velocity determined by the solution on the basis of the mass flux continuity. Accordingly, conditions at infinity should be supplemented as follows. Far from the inhomogeneity, the steady second-order potential behaves like a steady potential corresponding to a uniform current, namely

$$\text{(Ivii)} \qquad \frac{\partial\varphi_{20}(x,z)}{\partial x} \to u_{20}^{-\infty} \quad \text{as} \quad x \to -\infty,$$

and

$$\text{(Tiv)} \qquad \frac{\partial\varphi_{20}(x,z)}{\partial x} \to u_{20}^{+\infty} \quad \text{as} \quad x \to \infty,$$

where the velocities $u_{20}^{-\infty}$, $u_{20}^{+\infty}$ are unknown and will be obtained from the solution.

Conditions (Ivii) and (Tiv) constitute *the conditions at infinity of the steady problem.*

2.5. *Frequency-domain formulation of the linearized and second-order problems*

Substitution of (2.7) and (2.8) into the linearized and second-order problems results in the reformulation of the problems in the frequency domain, i.e. with respect to the potentials $\varphi_1(x, z)$ and $\varphi_{2r}(x, z)$, $r = 2, 0$. The complete formulation of the first- and second-order problems in the frequency domain is summarized in table 1.

The linearized problem can be efficiently solved in the whole domain D, by means of the consistent coupled-mode theory developed in AB. Having determined the first-order solution, we proceed to calculate the forcing terms in the second-order problem. These forcing terms include the forcing from infinity in the 2ω problem (components Iiii, Iiv, Iv and Tii), and the free-surface forcing terms $(F_{22}(x), \tilde{F}_{20}(x))$, given by the formulae

$$F_{22}(x) = \frac{\mathrm{i}\omega}{g}\left\{(\nabla\varphi_1(x,0))^2 - \frac{\varphi_1(x,0)}{2g}\left(-\omega^2\frac{\partial\varphi_1(x,0)}{\partial z} + g\frac{\partial^2\varphi_1(x,0)}{\partial z^2}\right)\right\}, \quad -\infty < x < \infty, \tag{2.9}$$

and

$$\tilde{F}_{20}(x) = -\frac{\mathrm{i}\omega}{2g^2}\bar{\varphi}_1(x,0)\left(-\omega^2\frac{\partial\varphi_1(x,0)}{\partial z} + g\frac{\partial^2\varphi_1(x,0)}{\partial z^2}\right), \quad -\infty < x < \infty, \tag{2.10}$$

where an overbar (here and in what follows) denotes the complex conjugate.

Since, however, Ξ^2 is real and, by (2.8*a*), we are interested only in the real part of the solution to the steady problem, we can simplify it by considering only the real part of its free-surface forcing:

$$F_{20}(x) = \mathrm{Re}\{\tilde{F}_{20}(x)\} = -\mathrm{Re}\left\{\frac{\mathrm{i}\omega}{2g}\bar{\varphi}_1(x,0)\frac{\partial^2\varphi_1(x,0)}{\partial z^2}\right\}, \quad -\infty < x < \infty. \tag{2.11}$$

To derive the right-hand side of the above equation, use was made of the fact that, on the free surface, $\mathrm{Re}(\mathrm{i}\bar{\varphi}_1\partial\varphi_1/\partial z) = \mathrm{Re}(\mathrm{i}\mu|\varphi_1|^2) = 0$. The solution to the steady problem is indeterminate up to a constant. We shall discuss the fixing of this constant in the next section, where we shall present the general representations of the second-order potentials $\varphi_{2r}(x,z)$, $r = 2, 0$, in the two constant-depth half-strips.

3. Energy flux and mass flux in the variable bathymetry region

The instantaneous energy flux past a vertical section at $x = \text{const.}$ is, by its definition, a second-order quantity. The leading term of its expansion is completely defined in terms of the linearized potential, as follows:

$$E(x,t) = \rho\int_{z=-h(x)}^{z=\eta(x;t)}\frac{\partial\Phi}{\partial t}\frac{\partial\Phi}{\partial x}\mathrm{d}z = \rho\varepsilon^2\int_{z=-h(x)}^{z=0}\frac{\partial\phi_1}{\partial t}\frac{\partial\phi_1}{\partial x}\mathrm{d}z + \text{higher order terms}, \tag{3.1}$$

see e.g. Stoker (1957, § 1.6), Wehausen & Laitone (1960, § 8). The time-average energy flux is also a second-order quantity, given by

$$E_{av}(x) = \frac{\rho g H^2}{8\omega}\int_{z=-h(x)}^{z=0}\mathrm{Im}\left\{\bar{\varphi}_1(x,z)\frac{\partial\varphi_1(x,z)}{\partial x}\right\}\mathrm{d}z + O(\varepsilon\Xi)^4. \tag{3.2}$$

Energy conservation leads, in the case of a left-incident wave, to the equation (Wehausen & Laitone 1960, § 17)

$$c_g^{(1)}(1 - |A_R|^2) = c_g^{(3)}|A_T|^2, \tag{3.3a}$$

where A_R is the reflection and A_T the transmission coefficient, and

$$c_g^{(j)} = \frac{\omega}{2k_0^{(j)}}\left(1 + \frac{2k_0^{(j)}h_j}{\sinh(2k_0^{(j)}h_j)}\right), \quad j = 1, 3, \tag{3.3b}$$

are the group velocities in the left ($D^{(1)}$) and right ($D^{(3)}$) half-strips. Similar relations also hold in the case of a right-incident wave, or a combined incidence, see e.g. Massel (1989), Porter & Chamberlain (1997). The next term in average energy flux E_{av} is of fourth order, $O(\varepsilon\Xi)^4$. Note that working up to the second order does not permit us to calculate the next term in the energy expansion (3.2), since the $(3,1)$ interaction terms are not available.

Let us now consider the mass flux through a vertical section in the variable bathymetry region,

$$M(x) = \rho \int_{z=-h(x)}^{z=\eta(x;t)} \frac{\partial \Phi(x,z;t)}{\partial x} \mathrm{d}z. \tag{3.4}$$

Using (2.5), (2.7), and (2.8) we easily obtain that the average mass flux through a vertical section in the variable bathymetry region is also a second-order quantity, with a leading term of the form

$$M_{av}(x) = M_{av}^{W}(x) + M_{av}^{C}(x) = \frac{\rho g H^2}{8\omega} \mathrm{Im}\left\{ \bar{\varphi}_1 \frac{\partial \varphi_1}{\partial x} \right\}_{z=0} - \frac{\rho g^2 H^2}{4\omega^2} \int_{z=-h(x)}^{z=0} \frac{\partial \varphi_{20}(x,z)}{\partial x} \mathrm{d}z. \tag{3.5}$$

In (3.5) M_{av}^{W} denotes the second-order mass flux component generated by the linearized wave potential, which corresponds to the mass transport due to the 'Stokes drift velocity', see e.g. Debnath (1994, § 2.9), Massel (1989, chap. 2.3). The other component, M_{av}^{C}, in the right-hand side of (3.5), is the second-order mass flux generated by the steady second-order potential φ_{20}, which corresponds to a uniform current at infinity. M_{av}^{W} and M_{av}^{C} will be called in what follows the *wave-generated* mass flux, and the *current-generated* mass flux, respectively. Differentiating the term $M_{av}^{W}(x)$ with respect to x we obtain

$$\begin{aligned} \frac{\mathrm{d}M_{av}^{W}(x)}{\mathrm{d}x} &= \frac{\rho g H^2}{8\omega} \mathrm{Im}\left\{ \bar{\varphi}_1 \frac{\partial^2 \varphi_1}{\partial x^2} \right\}_{z=0} \\ &= -\frac{\rho g H^2}{8\omega} \mathrm{Im}\left\{ \bar{\varphi}_1 \frac{\partial^2 \varphi_1}{\partial z^2} \right\}_{z=0} = \rho(\varepsilon\Xi)^2 F_{20}(x), \end{aligned} \tag{3.6}$$

where, for the derivation of the last equation, use was made of (2.11). By integrating (3.6) between two arbitrary points x_1 and $x_2 > x_1$, we obtain the following result concerning the wave-generated mass flux:

$$M_{av}^{W}(x_2) - M_{av}^{W}(x_1) = \rho(\varepsilon\Xi)^2 \int_{x=x_1}^{x=x_2} F_{20}(x)\mathrm{d}x. \tag{3.7}$$

From (3.5) and (3.7) we can see that in the case of a constant-depth strip, where $F_{20} = 0$, the wave-generated mass flux is constant; see also (2.2c).

In the case of the variable bathymetry strip D, the wave-generated mass flux $M_{av}^{W}(x)$ is non-constant along the horizontal axis, according to (3.7). To illustrate better this effect, let us consider the case of an abrupt underwater step, with different depths h_j, $j = 1, 3$, at infinity, see e.g. Massel (1989, chap. 3.5). In this case, the imbalance of the wave-generated mass flux at infinity is

$$M_{av}^{W}(+\infty) - M_{av}^{W}(-\infty) = \frac{\rho g H^2}{8\omega} \left(\mathrm{Im}\left\{ \bar{\varphi}_1 \frac{\partial \varphi_1}{\partial x} \right\}_{x=\infty} - \mathrm{Im}\left\{ \bar{\varphi}_1 \frac{\partial \varphi_1}{\partial x} \right\}_{x=-\infty} \right)_{z=0}, \tag{3.8a}$$

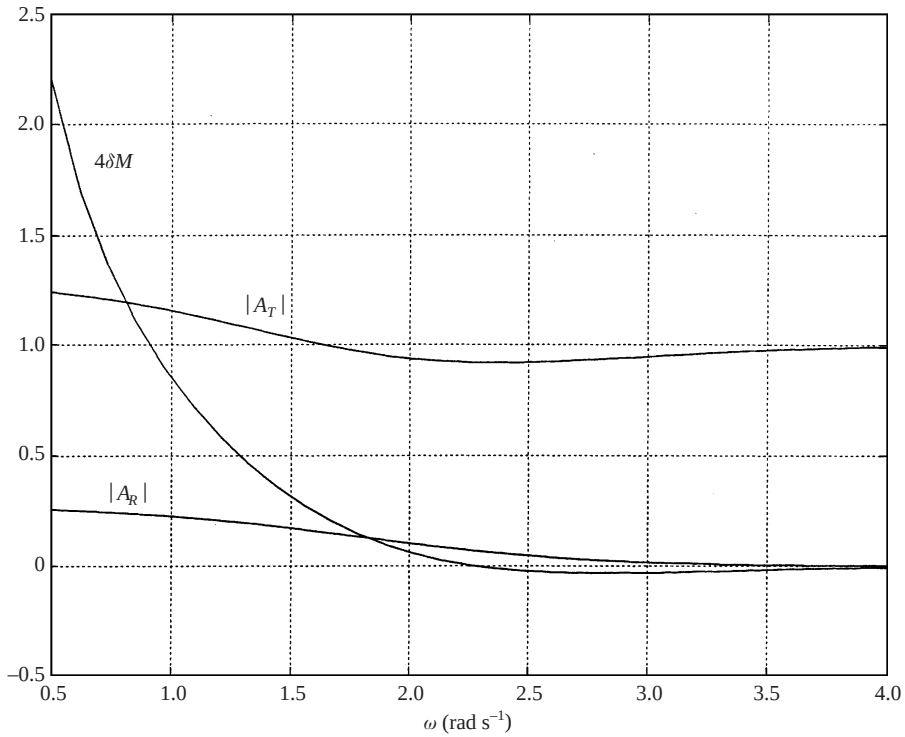

FIGURE 2. Reflection (A_R), transmission (A_T), and wave-generated mass imbalance (δM_{av}^W) coefficients vs. frequency ω, for a left-incident wave past an underwater step. Left-depth $h_1 = 6\,\mathrm{m}$, right-depth $h_3 = 2\,\mathrm{m}$. (Note that, for clarity, the curve $4\delta M_{av}^W$ has been plotted in the figure.)

which leads to the following wave-generated mass imbalance coefficient:

$$\delta M_{av}^W = \frac{M_{av}^W(+\infty) - M_{av}^W(-\infty)}{\rho\omega H^2} = \frac{g}{8\omega^2}(k_0^{(3)}|A_T|^2 - k_0^{(1)}(1 - |A_R|^2)). \tag{3.8b}$$

Comparing (3.8*b*) and (3.3) we see that δM_{av}^W is generally non-zero. Numerical results exhibiting the above effect are presented in figure 2 for an underwater step with depths $h_1 = 6\,\mathrm{m}$ and $h_3 = 2\,\mathrm{m}$, and for the range of frequencies from $\omega = 0.5\,\mathrm{rad\,s^{-1}}$ (globally shallow-water conditions for this environment) to $\omega = 4\,\mathrm{rad\,s^{-1}}$ (globally deep-water conditions). From this figure, we can clearly observe that the wave-generated mass imbalance can have positive or negative values, and its magnitude becomes higher at the lower frequencies. The same effect is also expected in the case of a smooth bottom profile joining two regions of constant but different depth at infinity.

We conclude this section by stating and proving the following theorem concerning the second-order mass flux balance in a variable bathymetry region:

THEOREM A. *Mass flux balance*: *The mass flux generated by the steady second-order potential $\varphi_{20}(x, z)$ in a variable bathymetry region, exactly balances the differences in the mass flux generated by the linearized wave potential $\varphi_1(x, z)$, so that the total mass flux $M_{av}(x)$,* (3.5)*, past any vertical section in the strip D remains constant* (*up to the second order*).

Proof. By using (3.5), in conjunction with Green's theorem applied to $\varphi_{20}(x,z)$ we obtain

$$M_{av}^{C}(x_2)-M_{av}^{C}(x_1)=-\frac{\rho g^2H^2}{4\omega^2}\left\{\int_{z=-h(x_2)}^{z=0}\frac{\partial\varphi_{20}(x_2,z)}{\partial x}\mathrm{d}z-\int_{z=-h(x_1)}^{z=0}\frac{\partial\varphi_{20}(x_1,z)}{\partial x}\mathrm{d}z\right\}$$

$$=\frac{\rho g^2H^2}{4\omega^2}\int_{x=x_1}^{x=x_2}\frac{\partial\varphi_{20}(x,z=0)}{\partial z}\mathrm{d}x=\frac{\rho g^2H^2}{4\omega^2}\int_{x=x_1}^{x=x_2}F_{20}(x)\mathrm{d}x$$

$$=-\rho(\varepsilon\Xi)^2\int_{x=x_1}^{x=x_2}F_{20}(x)\mathrm{d}x$$

$$=-(M_{av}^{W}(x_2)-M_{av}^{W}(x_1)), \tag{3.9}$$

and thus $M_{av}^{W}(x_1)+M_{av}^{C}(x_1)=M_{av}^{W}(x_2)+M_{av}^{C}(x_2)$, i.e. the average mass flux is completely balanced.

The above discussion clearly demonstrates the importance of including the steady second-order potential (induced current) in the solution of the second-order problem over variable bathymetry regions.

4. Decomposition of the second-order potentials and representations in the two half-strips $D^{(j)}$, $j=1,3$

The linearized problem has been formulated and solved, in AB, as a transmission problem in the bounded subdomain $D^{(2)}$, with the aid of normal-mode expansions in the two half-strips $D^{(j)}$, $j=1,3$, and a local-mode representation of the wave potential in the variable bathymetry subdomain $D^{(2)}$. In the present paper full use of all tools and results of AB will be made, with the goal of extending this theory to cover the second-order case. We, nevertheless, repeat herewith the following four formulae, in order to fix the notation and facilitate the introduction of the second-order counterparts. The general representations of the linearized wave potential $\varphi_1(x,z)$ in the two semi-infinite (constant-depth) strips $D^{(1)}$ and $D^{(3)}$ are

$$\varphi_1^{(1)}(x,z)=(A_0\exp(\mathrm{i}k_0^{(1)}x)+A_R\exp(-\mathrm{i}k_0^{(1)}x))Z_0^{(1)}(z)$$
$$+\sum_{n=1}^{\infty}C_n^{(1)}Z_n^{(1)}(z)\exp(k_n^{(1)}(x-a)),\quad (x,z)\in D^{(1)}, \tag{4.1a}$$

$$\varphi_1^{(3)}(x,z)=A_T\exp(\mathrm{i}k_0^{(3)}x)Z_0^{(3)}(z)+\sum_{n=1}^{\infty}C_n^{(3)}Z_n^{(3)}(z)\exp(k_n^{(3)}(b-x)),\quad (x,z)\in D^{(3)}. \tag{4.1b}$$

In the above expansions the terms $(A_0\exp(\mathrm{i}k_0^{(1)}x)+A_R\exp(-\mathrm{i}k_0^{(1)}x))Z_0^{(1)}(z)$ and $A_T\exp(\mathrm{i}k_0^{(3)}x)Z_0^{(3)}(z)$ define the *propagating modes*. The remaining terms ($n=1,2,\ldots$) are the *evanescent modes*. The sets of numbers $\{\mathrm{i}k_0^{(j)},k_n^{(j)},n=1,2,\ldots\}$, $j=1,3$, and the sets of functions $\{Z_n^{(j)}(z),n=0,1,2,\ldots\}$, $j=1,3$, are the eigenvalues and the corresponding eigenfunctions of the regular Sturm–Liouville problems obtained by separation of variables in the half-strips $D^{(j)}$, $j=1,3$. The eigenvalues $\{\mathrm{i}k_0^{(j)},k_n^{(j)}\}$ are obtained as the roots of the dispersion relations

$$\mu h_j=-k^{(j)}h_i\tan(k^{(j)}h_j),\quad j=1,3, \tag{4.2}$$

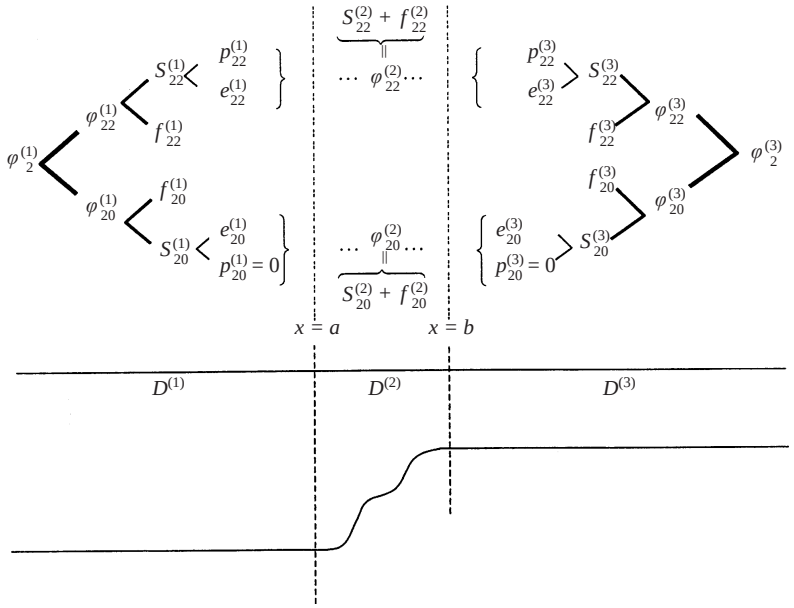

FIGURE 3. General scheme of the decomposition of the second-order potentials in the three subdomains. The vertical dashed lines indicate matching boundaries.

and the eigenfunctions $\{Z_n^{(j)}(z), n = 0, 1, 2, \ldots\}$ are given by

$$Z_0^{(j)}(z) = \frac{\cosh(k_0^{(j)}(z + h_j))}{\cosh(k_0^{(j)} h_j)}, \quad Z_n^{(j)}(z) = \frac{\cos(k_n^{(j)}(z + h_j))}{\cos(k_n^{(i)} h_j)}, \quad n = 1, 2, \ldots, \quad j = 1, 3. \tag{4.3}$$

The correctness (completeness) of the above expansions follows by the standard theory of regular eigenvalue problems, see e.g. Coddington & Levinson (1955, § 7.4).

Following a similar approach as for the linearized problem, the second-order problems will be treated by introducing domain decomposition, and reformulating them as matching boundary value problems in the finite (variable bathymetry) subdomain $D^{(2)}$. This is accomplished by means of semi-discrete, normal-mode representations of the second-order potentials $\varphi_{2r}^{(j)}(x, z)$, $r = 2, 0$, in the two half-strips $D^{(j)}$, $j = 1, 3$, and appropriate local-mode representations of $\varphi_{2r}^{(2)}(x, z)$, $r = 2, 0$, in $D^{(2)}$.

The general scheme of the decomposition of the second-order potentials in the three subdomains, and of our approach to the solution of the second-order problem, is illustrated in figure 3. As we can see in this figure, the second-order potentials in the two half-strips are decomposed into bound and free potentials, as follows:

$$\varphi_{2r}^{(j)}(x, z) = S_{2r}^{(j)}(x, z) + f_{2r}^{(j)}(x, z), \quad r = 2, 0, \quad j = 1, 3, \tag{4.4}$$

where $S_{2r}^{(j)}(x, z)$ are known functions representing particular solutions which satisfy the non-homogeneous free-surface conditions, and $f_{2r}^{(j)}(x, z)$ represents the general solution of the homogeneous problems in $D^{(j)}$, $j = 1, 3$. The particular solutions $S_{2r}^{(j)}(x, z)$ are further seen to contain a non-decaying at infinity (or propagating) part, which is denoted by $p_{2r}^{(j)}(x, z)$, and an evanescent part, which is denoted by $e_{2r}^{(j)}(x, z)$.

To establish the representation of the second-order potentials $\varphi_{2r}^{(2)}(x,z)$ in the variable bathymetry subdomain $D^{(2)}$, a similar decomposition as in the two half-strips is applied, also expressed by (4.4) with $j=2$. In this case, although $S_{2r}^{(2)}(x,z)$ are constructed to satisfy the (corresponding) non-homogeneous free-surface conditions in $D^{(2)}$, they are not particular solutions, since they do not satisfy the Laplace equation and the bottom boundary condition there. The problem is treated by providing the unknown component $f_{22}^{(2)}(x,z)$ with all appropriate conditions, so that the superposition $S_{22}^{(2)}(x,z)+f_{22}^{(2)}(x,z)$ satisfies all requirements of the second-order problems, and ensuring the matching at the interfaces, at $x=a$ and $x=b$. More details will be provided in § 4.3 below.

4.1. *General representations of the wave potential $\varphi_{22}(x,z)$ in the two half-strips*

The general representation of the wave potential $\varphi_{22}(x,z)$ in a constant-depth strip has been presented by several authors, see e.g. Massel (1983), Hudspeth & Sulisz (1991), Sulisz (1993). For completeness, we shall recapitulate these representations below, in the two half-strips $D^{(j)}$, $j=1,3$, of constant depths h_j, respectively. The only difference between the formulae given below and the ones presented by the above authors is the term corresponding to the incident second-harmonic component (Iv) in the left half-strip, which is included in our formulation as forcing from infinity to the 2ω problem.

The 2ω wave potential $\varphi_{22}^{(1)}(x,z)$ in the left strip $D^{(1)}$ is decomposed as follows:

$$\varphi_{22}^{(1)}(x,z)=S_{22}^{(1)}(x,z)+f_{22}^{(1)}(x,z)=p_{22}^{(1)}(x,z)+e_{22}^{(1)}(x,z)+f_{22}^{(1)}(x,z). \tag{4.5}$$

The component $S_{22}^{(1)}(x,z)$, which represents a particular solution of the 2ω-problem satisfying the non-homogeneous free-surface condition, comprises second-order Stokes waves bound to the linearized solution in $D^{(1)}$, and is further subdivided into the propagating Stokes waves $p_{22}^{(1)}$ and the evanescent ones $e_{22}^{(1)}$, defined by

$$p_{22}^{(1)}=\lambda_{0R}+(\lambda_0\exp(2\mathrm{i}k_0^{(1)}x)+\lambda_R\exp(-2\mathrm{i}k_0^{(1)}x))\cosh[2k_0^{(1)}(z+h_1)], \tag{4.6a}$$

$$\begin{aligned} e_{22}^{(1)}=&\sum_{n=1}^{\infty}\lambda_{0n}\exp[(k_n^{(1)}+\mathrm{i}k_0^{(1)})x]\cos[(k_n^{(1)}+\mathrm{i}k_0^{(1)})(z+h_1)]\\ &+\sum_{n=1}^{\infty}\lambda_{Rn}\exp[(k_n^{(1)}-\mathrm{i}k_0^{(1)})x]\cos[(k_n^{(1)}-\mathrm{i}k_0^{(1)})(z+h_1)]\\ &+\sum_{m=1}^{\infty}\sum_{n=1}^{\infty}\lambda_{mn}^{(1)}\exp[(k_m^{(1)}+k_n^{(1)})x]\cos[(k_m^{(1)}+k_n^{(1)})(z+h_1)]. \end{aligned} \tag{4.6b}$$

The coefficients λ_{0R}, λ_0, λ_R, λ_{0n}, λ_{Rn}, and $\lambda_{mn}^{(1)}$, $n,m=1,2,3,\ldots$, appearing in the above expansions are not dependent on the spatial variables (x,z) and are given in Appendix A. They all are expressed in terms of the solution of the linearized problem and, thus, they are considered as known quantities.

The component $f_{22}^{(1)}(x,z)$, which represents the general solution of the homogeneous 2ω-problem in $D^{(1)}$, comprises free second-order waves in the left half-strip, and also

includes propagating and evanescent parts, as follows:

$$f_{22}^{(1)}(x,z) = (\Lambda_0 \exp(\mathrm{i}\kappa_0^{(1)}x) + \Lambda_R \exp(-\mathrm{i}\kappa_0^{(1)}x))z_0^{(1)}(z) + \sum_{n=1}^{\infty} \Lambda_n^{(1)} z_n^{(1)}(z) \exp(\kappa_n^{(1)}(x-a)),$$
$$(x,z) \in D^{(1)}. \quad (4.7)$$

In (4.7) the set of numbers $\{\mathrm{i}\kappa_0^{(1)}, \kappa_n^{(1)}, n = 1,2,\ldots\}$, and the set of vertical functions $\{z_n^{(1)}(z), n = 0,1,2,\ldots\}$, are the eigenvalues and the corresponding eigenfunctions of a regular Sturm–Liouville problem in $[-h_1, 0]$ with frequency parameter $\mu_2 = 4\mu$. Thus, the eigenvalues $\{\mathrm{i}\kappa_0^{(1)}, \kappa_n^{(1)}, n = 1,2,\ldots\}$ are obtained as the roots of the dispersion relation (4.2) for $j = 1$ and $\mu = \mu_2$, and the corresponding eigenfunctions $\{z_n^{(1)}(z), n = 0,1,2,\ldots\}$ are defined by (4.3) with the $k_n^{(1)}$ being replaced by $\kappa_n^{(1)}$. The coefficient Λ_0 is known from the incident wave system. The coefficients Λ_R, $\{\Lambda_n^{(1)}\}_{n=1,2,\ldots}$ constitute the degrees of freedom of representation (4.5) and will be determined through the solution of the 2ω problem.

Similarly, the 2ω wave potential in the right half-strip $D^{(3)}$ is decomposed as follows:

$$\varphi_{22}^{(3)}(x,z) = S_{22}^{(3)}(x,z) + f_{22}^{(3)}(x,z) = p_{22}^{(3)}(x,z) + e_{22}^{(3)}(x,z) + f_{22}^{(3)}(x,z), \quad (4.8)$$

where

$$p_{22}^{(3)} = \lambda_T \exp(2\mathrm{i}k_0^{(3)}x)\cosh[2k_0^{(3)}(z+h_3)], \quad (4.9a)$$

$$e_{22}^{(3)} = \sum_{n=1}^{\infty} \lambda_{Tn} \exp[(\mathrm{i}k_0^{(3)} - k_n^{(3)})x] \cos[(k_n^{(3)} - \mathrm{i}k_0^{(3)})(z+h_3)]$$
$$+ \sum_{m=1}^{\infty}\sum_{n=1}^{\infty} \lambda_{mn}^{(3)} \exp[-(k_m^{(3)} + k_n^{(3)})x] \cos[(k_m^{(3)} + k_n^{(3)})(z+h_3)], \quad (4.9b)$$

$$f_{22}^{(3)}(x,z) = \Lambda_T \exp(\mathrm{i}\kappa_0^{(3)}x) z_0^{(3)}(z) + \sum_{n=1}^{\infty} \Lambda_n^{(3)} z_n^{(3)}(z) \exp(\kappa_n^{(3)}(b-x)), \quad (x,z) \in D^{(3)}. \quad (4.10)$$

The coefficients λ_T, λ_{Tn} and $\lambda_{mn}^{(3)}$, $n,m = 1,2,3,\ldots$, appearing in (4.9), are known (through the linearized solution), and are given in Appendix A. As previously, the eigenvalues $\{\mathrm{i}\kappa_0^{(3)}, \kappa_n^{(3)}, n = 1,2,\ldots\}$, appearing in (4.10), are obtained as the roots of the dispersion relation (4.2) for $j = 3$ and $\mu = \mu_2$, and the corresponding eigenfunctions $\{z_n^{(3)}(z), n = 0,1,2,\ldots\}$ are given by (4.3) with the $k_n^{(3)}$ being replaced by $\kappa_n^{(3)}$. The coefficients $\Lambda_T, \{\Lambda_n^{(3)}\}_{n=1,2,\ldots}$ constitute the degrees of freedom of the representation (4.8) and will be determined through the solution of the 2ω problem.

4.2. *General representations of the steady wave potential $\varphi_{20}(x,z)$ in the two half-strips*

The general representation of the steady wave potential $\varphi_{20}(x,z)$ is obtained in a similar way as the representation of $\varphi_{22}(x,z)$, see e.g. Hudspeth & Sulisz (1991). The potential $\varphi_{20}^{(1)}(x,z)$, in the left half-strip $D^{(1)}$, can be decomposed into two parts as follows:

$$\varphi_{20}^{(1)}(x,z) = S_{20}^{(1)}(x,z) + f_{20}^{(1)}(x,z) = e_{20}^{(1)}(x,z) + f_{20}^{(1)}(x,z). \quad (4.11)$$

The component $S_{20}^{(1)}(x,z) = e_{20}^{(1)}(x,z)$ represents a particular solution of the steady problem satisfying the non-homogeneous free-surface condition. It comprises only

evanescent terms ($p_{20}^{(1)}(x,z)=0$), and is given by

$$e_{20}^{(1)}(x,z)=\mathrm{Re}\Bigg\{\sum_{m=1}^{\infty}\tilde{\gamma}_{Rn}\exp[(k_n^{(1)}+\mathrm{i}k_0^{(1)})x]\cos[(k_n^{(1)}+\mathrm{i}k_0^{(1)})(z+h_1)]$$
$$+\sum_{n=1}^{\infty}\gamma_{Rn}\exp[(k_n^{(1)}-\mathrm{i}k_0^{(1)})x]\cos[(k_n^{(1)}-\mathrm{i}k_0^{(1)})(z+h_1)]$$
$$+\sum_{m=1}^{\infty}\sum_{\substack{n=1\\(n\neq m)}}^{\infty}\gamma_{mn}^{(1)}\exp[(k_m^{(1)}+k_n^{(1)})x]\cos[(k_m^{(1)}+k_n^{(1)})(z+h_1)]\Bigg\}. \tag{4.12}$$

The coefficients $\tilde{\gamma}_{Rn}$, γ_{Rn}, $\gamma_{mn}^{(1)}$, $n,m=1,2,3,\ldots$, appearing in the above expansion, are determined through the linearized potential in $D^{(1)}$, and are given in Appendix A.

The component $f_{20}^{(1)}(x,z)$ in (4.11) represents the general solution to the homogeneous steady problem in $D^{(1)}$, and is given by

$$f_{20}^{(1)}(x,z)=\Gamma_0^{(1)}(x-a)T_0^{(1)}(z)+\sum_{n=1}^{\infty}\Gamma_n^{(1)}T_n^{(1)}(z)\exp\left(\frac{n\pi(x-a)}{h_1}\right),\quad (x,z)\in D^{(1)}, \tag{4.13a}$$

where the set of vertical functions $\{T_n^{(1)}(z)\}_{n=0,1,2,\ldots}$ involved in (4.13a) is

$$\left\{T_0^{(1)}(z)=1,\quad T_n^{(1)}(z)=\cos\left(\frac{n\pi z}{h_1}\right),\quad n=1,2,\ldots\right\}. \tag{4.13b}$$

The completeness of the representation (4.13a) follows from the basis properties of the set (4.13b). We note here that the most general form of the first term in (4.13a) is of the form $\Gamma_0^{(1)}(x-\Gamma_*^{(1)})$, where $\Gamma_0^{(1)}$ and $\Gamma_*^{(1)}$ are two undetermined constants. However, only $\Gamma_0^{(1)}$ is essential, describing the behaviour at infinity ($x\to-\infty$) of $\varphi_{20}^{(1)}(x,z)$; in fact, $\Gamma_0^{(1)}=u_{20}^{-\infty}$. The second, inessential, constant $\Gamma_*^{(1)}$ has been arbitrarily selected to be equal to a, the abscissa of the right-hand end of the half-strip $D^{(1)}$.

The steady wave potential in the right half-strip is similarly decomposed:

$$\varphi_{20}^{(3)}(x,z)=S_{20}^{(3)}(x,z)+f_{20}^{(3)}(x,z)=e_{20}^{(3)}(x,z)+f_{20}^{(3)}(x,z). \tag{4.14}$$

Now $S_{20}^{(3)}(x,z)=e_{20}^{(3)}(x,z)$ is given by

$$e_{20}^{(3)}(x,z)=\mathrm{Re}\Bigg\{\sum_{n=1}^{\infty}\tilde{\gamma}_{Tn}\exp[-(k_n^{(3)}+\mathrm{i}k_0^{(3)})x]\cos[(k_n^{(3)}+\mathrm{i}k_0^{(3)})(z+h_3)]$$
$$+\sum_{n=1}^{\infty}\gamma_{Tn}\exp[-(k_n^{(3)}-\mathrm{i}k_0^{(3)})x]\cos[(k_n^{(3)}-\mathrm{i}k_0^{(3)})(z+h_3)]$$
$$+\sum_{m=1}^{\infty}\sum_{\substack{n=1\\(n\neq m)}}^{\infty}\gamma_{mn}^{(3)}\exp[-(k_m^{(3)}+k_n^{(3)})x]\cos[(k_m^{(3)}+k_n^{(3)})(z+h_3)]\Bigg\}, \tag{4.15}$$

where the coefficients $\tilde{\gamma}_{Tn}$, γ_{Tn} and $\gamma_{mn}^{(3)}$, $n,m=1,2,3,\ldots$, are determined through the linearized potential in $D^{(3)}$, and are given in Appendix A.

The component $f_{20}^{(3)}(x,z)$ is now given by

$$f_{20}^{(3)}(x,z) = (\Gamma_0^{(3)} + (\xi\Gamma_0^{(1)} + \nu)(x-b))T_0^{(3)}(z) + \sum_{n=1}^{\infty} \Gamma_n^{(3)} T_n^{(3)}(z) \exp\left(\frac{n\pi(b-x)}{h_3}\right), \quad (x,z) \in D^{(3)}, \tag{4.16a}$$

where the vertical basis

$$\{T_n^{(3)}(z)\}_{n=0,1,2,\ldots} = \left\{ T_0^{(3)}(z) = 1, \quad T_n^{(3)}(z) = \cos\left(\frac{n\pi z}{h_3}\right), \quad n = 1,2,\ldots \right\}.$$

The first term of the right-hand side of (4.16*a*) needs some explanation. In principle, its general form is $\Delta_0^{(3)}(x - \Delta_*^{(3)})$, similarly to the left half-strip, where $\Delta_0^{(3)}$ and $\Delta_*^{(3)}$ are two undetermined constants. Now, however, both constants are essential, $\Delta_0^{(3)}$ describing the behaviour at infinity ($x \to +\infty$) of $\varphi_{20}^{(3)}(x,z)$ (in fact $\Delta_0^{(3)} = u_{20}^{+\infty}$), and $\Delta_0^{(3)}\Delta_*^{(3)}$ being a blockage constant. There is, however, a relation among $\Delta_0^{(3)}$, $\Delta_*^{(3)}$ and $\Gamma_0^{(1)}$ (the undetermined constant of the left half-strip), obtained by applying Green's theorem to $\varphi_{20}(x,z)$ in the whole domain D (in a limiting sense). Using this relation we can rewrite the term $\Delta_0^{(3)}(x - \Delta_*^{(3)})$ in the form $(\Gamma_0^{(3)} + (\xi\Gamma_0^{(1)} + \nu)(x-b))T_0^{(3)}(z)$, where $\Gamma_0^{(3)}$ is the new undetermined constant, and ξ, ν are given as

$$\xi = h_1/h_3, \quad \nu = -\frac{1}{h_3}\int_{x=-\infty}^{x=\infty} F_{20}(x)\mathrm{d}x. \tag{4.16b}$$

The convergence of the integral is guaranteed, since the steady forcing $F_{20}(x)$ exhibits an exponential decay at infinity, as can be easily verified using (2.11) in conjunction with the representations (4.1) and (4.2).

4.3. *Decomposition of the second-order potentials in $D^{(2)}$*

To proceed with the reformulation of the second-order problems as transmission problems in the variable bathymetry subdomain $D^{(2)}$, it was found convenient to introduce the following decomposition of the second-order wave potential $\varphi_{22}^{(2)}(x,z), (x,z) \in D^{(2)}$:

$$\varphi_{22}^{(2)}(x,z) = S_{22}^{(2)}(x,z) + f_{22}^{(2)}(x,z), \quad a \leqslant x \leqslant b, \quad -h_2(x) \leqslant z \leqslant 0, \tag{4.17a}$$

where $S_{22}^{(2)}(x,z)$ is a specific function (given below) satisfying the non-homogeneous free-surface condition of the 2ω problem in $D^{(2)}$ (although violating both the Laplace equation and the bottom boundary condition there), and $f_{22}^{(2)}(x,z)$ is an unknown component which will be provided with all appropriate conditions, so that the superposition $S_{22}^{(2)}(x,z) + f_{22}^{(2)}(x,z)$, satisfies the 2ω problem. In (4.17*a*) and in what follows, the symbol $h_2 = h_2(x)$ will be used to denote the x-dependent depth in the subdomain $D^{(2)}$.

One possible choice for $S_{22}^{(2)}(x,z)$ is

$$S_{22}^{(2)}(x,z) = F_{22}(x) z_{-2}^{(2)}(z;x), \text{ with } z_{-2}^{(2)}(z;x) = \frac{\cosh[2k_0^{(2)}(z+h_2(x))]}{2k_0^{(2)}\sinh(2k_0^{(2)}h_2(x)) - \mu_2\cosh(2k_0^{(2)}h_2(x))}, \tag{4.17b}$$

where $k_0^{(2)} = k_0^{(2)}(x)$ denotes the propagating wavenumber obtained as the root of the local (linearized) dispersion relation in $D^{(2)}$,

$$\omega^2 = k_0^{(2)} g \tanh(k_0^{(2)} h_2(x)), \quad a \leqslant x \leqslant b. \tag{4.18}$$

A similar decomposition is introduced in the steady second-order potential $\varphi_{20}^{(2)}(x,z)$, in $D^{(2)}$, namely

$$\varphi_{20}^{(2)}(x,z) = S_{20}^{(2)}(x,z) + f_{20}^{(2)}(x,z), \quad a \leqslant x \leqslant b, \quad -h_2(x) \leqslant z \leqslant 0. \tag{4.19a}$$

Here $S_{20}^{(2)}(x,z)$ is defined as

$$S_{20}^{(2)}(x,z) = F_{20}(x)T_{-2}^{(2)}(z;x), \text{ with } T_{-2}^{(2)}(z;x) = [h_2(x)((1+z/h_2(x))^3 - (1+z/h_2(x))^2)], \tag{4.19b}$$

and $f_{20}^{(2)}(x,z)$ will be determined so that the superposition $S_{20}^{(2)}(x,z) + f_{20}^{(2)}(x,z)$ satisfies the steady second-order problem.

Further comments regarding the rationale underlying the decompositions (4.17) and (4.19), and the specific choices for the vertical functions $z_{-2}^{(2)}(z,x)$ and $T_{-2}^{(2)}(z,x)$ will be given in § 6, where, also, the meaning of the subscript (-2) will be made clear, since the second-order wave potentials in $D^{(2)}$ will be expanded in local-mode series containing terms indexed by the set $\{-2,-1,0,1,2,\ldots\}$.

5. Reformulation of the second-order problems as transmission problems in $D^{(2)}$: variational formulation

Having constructed the representation of the second-order potentials in the two half-strips we are in a position to proceed to the reformulation of the second-order problems as transmission problems in $D^{(2)}$. For compactness in the presentation we introduce here the following notation: Let $C_{0,2}^{(1)}, \{C_{n,2}^{(1)}\}_{n\in N}$ denote the coefficients $\Lambda_R, \{\Lambda_n^{(1)}\}_{n\in N}$; $C_{0,2}^{(3)}, \{C_{n,2}^{(3)}\}_{n\in N}$ denote the coefficients $\Lambda_T, \{\Lambda_n^{(3)}\}_{n\in N}$; and $C_{0,1}^{(j)}, \{C_{n,1}^{(j)}\}_{n\in N}$ denote the coefficients $\Gamma_0^{(j)}, \{\Gamma_n^{(j)}\}_{n\in N}$, $j = 1,3$. With the aid of this notation we are able to unify the discussion for the two second-order potentials $\varphi_{22}^{(j)}$, $\varphi_{20}^{(j)}$, in the two half-strips $D^{(j)}$, $j = 1,3$, avoiding from now on separate presentations.

The half-strip potentials $f_{2r}^{(j)} = f_{2r}^{(j)}(x,z)$, $r = 2,0$, are uniquely determined in $D^{(j)}$, $j = 1,3$, in terms of the complex coefficients $C_{0,r}^{(j)}, \{C_{n,r}^{(j)}\}_{n\in N}$, respectively. Bearing this in mind we shall occasionally use the notation

$$f_{2r}^{(j)} = f_{2r}^{(j)}(x,z;C_{0,r}^{(j)},\{C_{n,r}^{(j)}\}_{n\in N}) \quad \text{or, simply,} \quad f_{2r}^{(j)} = f_{2r}^{(j)}(C_{0,r}^{(j)},\{C_{n,r}^{(j)}\}_{n\in N}), \quad r = 2,0, \quad j = 1,3.$$

By exploiting the decompositions (4.17) and (4.19), in conjunction with the representations (4.5) and (4.8) and (4.11) and (4.14), in the two half-strips, respectively, the second-order problems can be formulated as transmission boundary value problems in the bounded subdomain $D^{(2)}$, as follows:

Problems $\mathscr{P}_{T,2r}(D^{(2)})$, $r = 2,0$: Given (i) the linearized potential $\varphi_1(x,z)$ in D, (ii) the constant $\Lambda_0 = |\Lambda_0|\exp(\mathrm{i}\psi_0)$, where $|\Lambda_0| = O(1)$, and (iii) the representations (4.5) and (4.8), and (4.11) and (4.14) of the second-order potentials in the semi-infinite strips $D^{(1)}$ and $D^{(3)}$, find the coefficients $C_{0,r}^{(j)}, \{C_{n,r}^{(j)}\}_{n\in N}$, $r = 2,0$, $j = 1,3$, and the functions $f_{2r}^{(2)}(x,z)$, $r = 2,0$, in $D^{(2)}$, satisfying the following equations, and boundary and matching conditions:

$$\nabla^2 f_{2r}^{(2)} = -\nabla^2 S_{2r}^{(2)} \equiv g_r(x,z), \quad a < x < b, \quad h(x) < z < 0, \tag{5.1a}$$

$$\frac{\partial f_{2r}^{(2)}}{\partial n^{(2)}} - \delta_{2r}\mu_2 f_{2r}^{(2)} = 0, \quad a < x < b, \quad z = 0, \tag{5.1b}$$

$$\frac{\partial f_{2r}^{(2)}}{\partial n^{(2)}} = -\frac{\partial S_{2r}^{(2)}}{\partial n^{(2)}} \equiv b_r(x), \quad a < x < b, \quad z = -h(x), \tag{5.1c}$$

$$f_{2r}^{(2)} - f_{2r}^{(1)}(C_{0,r}^{(1)}, \{C_{n,r}^{(1)}\}_{n\in N}) = \delta_{2r} p_{2r}^{(1)} + e_{2r}^{(1)} - S_{2r}^{(2)} \equiv G_r^{(12)}(z), \quad x = a, \quad h(x) < z < 0, \tag{5.1d}$$

$$\frac{\partial f_{2r}^{(2)}}{\partial n^{(2)}} + \frac{\partial f_{2r}^{(1)}(C_{0,r}^{(1)}, \{C_{n,r}^{(1)}\}_{n\in N})}{\partial n^{(1)}} = -\frac{\partial S_{2r}^{(2)}}{\partial n^{(2)}} - \frac{\partial(\delta_{2r} p_{2r}^{(1)} + e_{2r}^{(1)})}{\partial n^{(1)}} \equiv \tilde{G}_r^{(12)}(z), \quad x = a, \quad h(x) < z < 0, \tag{5.1e}$$

$$f_{2r}^{(2)} - f_{2r}^{(3)}(C_{0,r}^{(3)}, \{C_{n,r}^{(3)}\}_{n\in N}) = \delta_{2r} p_{2r}^{(3)} + e_{2r}^{(3)} - S_{2r}^{(2)} \equiv G_r^{(23)}(z), \quad x = b, \quad h(x) < z < 0, \tag{5.1f}$$

$$\frac{\partial f_{2r}^{(2)}}{\partial n^{(2)}} + \frac{\partial f_{2r}^{(3)}(C_{0,r}^{(3)}, \{C_{n,r}^{(3)}\}_{n\in N})}{\partial n^{(3)}} = -\frac{\partial S_{2r}^{(2)}}{\partial n^{(2)}} - \frac{\partial(\delta_{2r} p_{2r}^{(3)} + e_{2r}^{(3)})}{\partial n^{(3)}} \equiv \tilde{G}_r^{(23)}(z), \quad x = b, \quad h(x) < z < 0, \tag{5.1g}$$

where $\boldsymbol{n}^{(j)} = (n_x^{(j)}, n_z^{(j)})$ is the unit normal vector to the boundary $\partial D^{(j)}$ directed to the exterior of $D^{(j)}$, $j = 1, 2, 3$, and δ_{pr} is Kronecker's delta. The terms $g_r(x, z)$, $b_r(x)$, $G_r^{(12)}(z)$, $\tilde{G}_r^{(12)}(z)$, $G_r^{(23)}(z)$ and $\tilde{G}_r^{(23)}(z)$, appearing on the right-hand side of the above equations, are known (in terms of the data (i), (ii) and (iii), described at the beginning of the problems statement) and represent forcing terms of the problems $\mathscr{P}_{T,2r}(D^{(2)})$. The forcing terms $g_r(x, z)$ and $b_r(x)$ ensure that the functions $f_{2r}^{(2)}(x, z)$, $r = 2, 0$ (the solutions to the problems $\mathscr{P}_{T,2r}$), cancel out the errors produced in the Laplace equation and in the bottom boundary condition by the prespecified fields $S_{2r}^{(2)}(x, z)$ (which served the purpose of making the free-surface boundary condition homogeneous; see (5.1*b*). Moreover, the jump conditions, (5.1*d*, *e*, *f*, *g*), are appropriately defined in order to ensure continuity of the second-order potentials $\varphi_{2r}(x, z)$, $r = 2, 0$, across the vertical interfaces at $x = a$ and $x = b$.

The two problems (5.1*a*–*g*) will be referred to as *the second-order transmission problems* $\mathscr{P}_{T,2r}(D^{(2)})$, $r = 2, 0$. These problems admit equivalent variational formulations, similar to the corresponding variational formulation of the linearized problem presented in AB. The appropriate functionals (for $r = 2, 0$) are

$$\begin{aligned}
&\mathscr{F}_r(f_{2r}^{(2)}(x, z), \{C_{n,r}^{(j)}\}_{n=0,1,2,\ldots}^{j=1,3}) \\
&\quad = \frac{1}{2}\int_{D^{(2)}} (\nabla f_{2r}^{(2)} + \nabla S_{2r}^{(2)})^2 \mathrm{d}V - \int_{\partial D_F^{(2)}} \left(\frac{\delta_{2r}\mu_2}{2}(f_{2r}^{(2)} + S_{2r}^{(2)})^2 + f_{2r} S_{2r}^{(2)} \right) \mathrm{d}S \\
&\qquad + \int_{\partial D_I^{(12)}} \left\{ (f_{2r}^{(2)} - G_r^{(12)}) \frac{\partial(f_{2r}^{(1)}(\{C_{n,r}^{(1)}\}_{n=0,1,2,\ldots}) + \delta_{2r} p_{2r}^{(1)} + e_{2r}^{(1)})}{\partial n^{(1)}} \right. \\
&\qquad\qquad \left. - \frac{1}{2} f_{2r}^{(1)}(\{C_{n,r}^{(1)}\}_{n=0,1,2,\ldots}) \frac{\partial f_{2r}^{(1)}(\{C_{n,r}^{(1)}\}_{n=0,1,2,\ldots})}{\partial n^{(1)}} \right\} \mathrm{d}S \\
&\qquad + \int_{\partial D_I^{(23)}} \left\{ (f_{2r}^{(2)} - G_r^{(23)}) \frac{\partial(f_{2r}^{(3)}(\{C_{n,r}^{(3)}\}_{n=0,1,2,\ldots}) + \delta_{2r} p_{2r}^{(3)} + e_{2r}^{(3)})}{\partial n^{(3)}} \right. \\
&\qquad\qquad \left. - \frac{1}{2} f_{2r}^{(3)}(\{C_{n,r}^{(3)}\}_{n=0,1,2,\ldots}) \frac{\partial f_{2r}^{(3)}(\{C_{n,r}^{(3)}\}_{n=0,1,2,\ldots})}{\partial n^{(3)}} \right\} \mathrm{d}S \\
&\qquad + \delta_{2r} \Lambda_0 C_{0,r}^{(1)} J^{(1)},
\end{aligned} \tag{5.2a}$$

where $J^{(1)}$ is a constant defined by the equation

$$J^{(1)} = \kappa_0^{(1)} \int_{z=-h_1}^{z=0} (z_0^{(1)}(z))^2 \mathrm{d}z. \tag{5.2b}$$

Using these functionals we can state the following.

THEOREM B. *The variational formulation of the second-order problems* $\mathscr{P}_{T,2r}$: *The functions* $f_{2r}^{(2)}(x,z)$, $(x,z) \in D^{(2)}$, *and the sets of coefficients* $C_{0,r}^{(j)}, \{C_{n,r}^{(j)}\}_{n\in N}$, $j = 1,3$, *satisfy equations* (5.1) *of the second-order transmission problems* $(r = 2,0)$, *if and only if they render the corresponding functionals* $\mathscr{F}_r$ *stationary, that is*

$$\delta\mathscr{F}_r(f_{2r}^{(2)}(x,z), \{C_{n,r}^{(1)}\}_{n=0,1,2,\ldots}, \quad \{C_{n,r}^{(3)}\}_{n=0,1,2,\ldots}) = 0, \quad r = 2,0. \tag{5.3a}$$

Sketch of Proof: By calculating the first variaiton $\delta\mathscr{F}_r$ of the functionals (5.1), we obtain the following variational equation:

$$\begin{aligned}
&-\int_{D^{(2)}} (\nabla^2 f_{2r}^{(2)} - g_r)\delta f_{2r}^{(2)} \mathrm{d}V + \int_{\partial D_H^{(2)}} \left(\frac{\partial f_{2r}^{(2)}}{\partial n^{(2)}} - b_r\right) \delta f_{2r}^{(2)} \mathrm{d}S \\
&+ \int_{\partial D_F^{(2)}} \left(\frac{\partial f_{2r}^{(2)}}{\partial n^{(2)}} - \delta_{2r}\mu_2 f_{2r}^{(2)}\right) \delta f_{2r}^{(2)} \mathrm{d}S \\
&+ \int_{\partial D_I^{(12)}} \left(\frac{\partial f_{2r}^{(1)}}{\partial n^{(1)}} + \frac{\partial f_{2r}^{(2)}}{\partial n^{(2)}} - \tilde{G}_r^{(12)}\right) \delta f_{2r}^{(2)} \mathrm{d}S \\
&+ \int_{\partial D_I^{(23)}} \left(\frac{\partial f_{2r}^{(2)}}{\partial n^{(2)}} + \frac{\partial f_{2r}^{(3)}}{\partial n^{(3)}} - \tilde{G}_r^{(23)}\right) \delta f_{2r}^{(2)} \mathrm{d}S \\
&+ \int_{\partial D_I^{(12)}} (f_{2r}^{(2)} - f_{2r}^{(1)} - G_r^{(12)})\delta \left(\frac{\partial f_{2r}^{(1)}}{\partial n^{(1)}}\right) \mathrm{d}S \\
&+ \int_{\partial D_I^{(23)}} (f_{2r}^{(2)} - f_{2r}^{(3)} - G_r^{(23)})\delta \left(\frac{\partial f_{2r}^{(3)}}{\partial n^{(3)}}\right) \mathrm{d}S = 0, \quad r = 2,0,
\end{aligned} \tag{5.3b}$$

In (5.3*b*), the term $\partial f_{2r}^{(2)}/\partial n^{(2)}$ on the bottom surface can be expressed in the form

$$\frac{\partial f_{2r}^{(2)}}{\partial n^{(2)}} = -\left(\frac{\partial f_{2r}^{(2)}}{\partial z} + \frac{\mathrm{d}h}{\mathrm{d}x}\frac{\partial f_{2r}^{(2)}}{\partial x}\right) \frac{1}{\sqrt{1 + (\mathrm{d}h_2/\mathrm{d}x)^2}}, \quad r = 2,0. \tag{5.4}$$

The variations $\delta(\partial f_{2r}^{(1)}/\partial n^{(1)})$ and $\delta(\partial f_{2r}^{(3)}/\partial n^{(3)})$ should be considered in terms of the variations $\delta C_{n,r}^{(j)}$, $j = 1,3$, as obtained with the aid of expansions (4.5) and (4.11) for $j = 1$, and (4.8) and (4.14) for $j = 3$. The proof of the equivalence of the variational equations (5.3) and the transmission problems (5.1) is completed by using standard arguments of the calculus of variations; see AB for a similar proof concerning the linearized problem in the variable bathymetry region.

The above variational principles will be used in § 7 for the derivation of equivalent coupled-mode systems of horizontal equations, after introducing consistent local-mode representations of the second order wave potentials $f_{2r}^{(2)}(x,z)$, $r = 2,0$, in $D^{(2)}$, in the next section.

6. Local-mode representations of the second-order potentials in the variable bathymetry region

A consistent local-mode representation for the linearized wave potential $\varphi_1(x,z)$ in the variable bathymetry subdomain $D^{(2)}$, first introduced in AB, is given by

$$\varphi_1^{(1)}(x,z) = \varphi_{-1}(x)Z_{-1}^{(2)}(z;x) + \varphi_0(x)Z_0^{(2)}(z;x) + \sum_{n=1}^{\infty} \varphi_n(x)Z_n^{(2)}(z;x). \tag{6.1}$$

In (6.1) the term $\varphi_0^{(2)}(x)Z_0^{(2)}(z;x)$ is the (linearized) propagating mode. The remaining terms $\varphi_n^{(2)}(x)Z_n^{(2)}(z;x)$, $n = 1,2,\ldots$ are the *evanescent modes*, and the additional term $\varphi_{-1}^{(2)}(x)Z_{-1}^{(2)}(z;x)$ is a correction term called the *sloping-bottom mode*, accounting for the boundary condition on a sloping bottom. The conditions that $Z_{-1}(z;x)$ should satisfy are described in AB. Note that $Z_{-1}(z;x)$ is not uniquely defined; however, this freedom does not affect the final results. For an extensive discussion about this issue the reader is referred to AB, §4. The rest of the vertical functions $Z_n^{(2)}(z;x)$, $n = 0,1,2,\ldots$, in (6.1) are obtained as the eigenfunctions of local vertical *Sturm–Liouville* problems, and are given by

$$\begin{aligned} Z_0^{(2)}(z;x) &= \frac{\cosh[k_0^{(2)}(x)(z+h_2(x))]}{\cosh(k_0^{(2)}(x)h_2(x))}, \\ Z_n^{(2)}(z;x) &= \frac{\cos[k_n^{(2)}(x)(z+h_2(x))]}{\cos(k_n^{(2)}(x)h_2(x))}, \quad n = 1,2,\ldots, \end{aligned} \tag{6.2a}$$

where the eigenvalues $\{ik_0^{(2)}(x), k_n^{(2)}(x)\}$ are obtained as the roots of the dispersion relation

$$\mu h_2(x) = -k(x)h_2(x)\tan[k(x)h_2(x)], \quad a \leqslant x \leqslant b. \tag{6.2b}$$

A specific, convenient form of the function $Z_{-1}^{(2)}(z;x)$, which is used in this work (§8) to obtain numerical results, is

$$Z_{-1}^{(2)}(z;x) = h_2(x)\left[\left(\frac{z}{h_2(x)}\right)^3 + \left(\frac{z}{h_2(x)}\right)^2\right]. \tag{6.2c}$$

Representation (6.1) is then used, in conjunction with the variational principle for the linearized problem, to derive the following coupled-mode system of equations, with respect to the modal amplitudes $\varphi_n(x)$, $n = -1,0,1,2,\ldots$:

$$\sum_{n=-1}^{\infty} a_{mn}(x)\frac{\mathrm{d}^2\varphi_n(x)}{\mathrm{d}x^2} + b_{mn}(x)\frac{\mathrm{d}\varphi_n}{\mathrm{d}x}(x) + c_{mn}(x)\varphi_n(x) = 0, \qquad a < x < b, \quad m = -1,0,1,\ldots, \tag{6.3}$$

supplemented by appropriate boundary conditions at the ends $x = a$ and $x = b$ of the variable bathymetry subdomain $D^{(2)}$; see AB, §5. These boundary conditions ensure the complete matching of the linearized wave potential $\varphi_1^{(2)}(x,z)$ with the representations (4.1*a*) for $\varphi_1^{(1)}(x,z)$ and (4.1*b*) for $\varphi_1^{(3)}(x,z)$, in the two half-strips, respectively. In what follows, this line of thought will be extended to the second-order problems.

6.1. *Representation of the second-order wave potential in the variable bathymetry region*

Owing to the decomposition (4.17), the second-order wave potential $f_{22}^{(2)}(x,z)$ satisfies the homogeneous free-surface boundary condition, ((5.1b) with $r=2$), in $D^{(2)}$. Consequently, the concept of the enhanced local-mode representation (see AB, § 4) can be applied once again to $f_{22}^{(2)}(x,z)$, leading to

$$f_{22}^{(2)}(x,z) = f_{-1,2}(x)z_{-1}^{(2)}(z;x) + \sum_{n=0}^{\infty} f_{n,2}(x)z_n^{(2)}(z;x) = \sum_{n=-1}^{\infty} f_{n,2}(x)z_n^{(2)}(z;x), \quad -h_2(x) \leqslant z \leqslant 0, \quad a \leqslant x \leqslant b, \quad (6.4)$$

where $f_{n,2}(x)$, $n=-1,0,1,\ldots$, denote the modal amplitudes of the second-order wave potential $f_{22}^{(2)}(x,z)$. The set of functions $\{z_n^{(2)}(z;x)\}$, $n=0,1,2,\ldots$, involved in the above representation is obtained as the solution of local Sturm–Liouville problems, formulated at the local depth $h_2(x)$ in $D^{(2)}$, satisfying the homogeneous free-surface condition for the second-order frequency parameter μ_2:

$$z_0^{(2)}(z;x) = \frac{\cosh[\kappa_0^{(2)}(z+h_2(x))]}{\cosh(\kappa_0^{(2)}(x)h_2(x))}, \quad z_n^{(2)}(z;x) = \frac{\cos[\kappa_n^{(2)}(x)(z+h_2(x))]}{\cos(\kappa_n^{(2)}(x)h_2(x))}, \quad n=1,2,\ldots,$$

where the eigenvalues $\{\mathrm{i}\kappa_0^{(2)}(x), \kappa_n^{(2)}(x)\}$ are obtained as the roots of the second-order dispersion relation formulated at the local depth, ((6.2b), with μ being replaced by μ_2).

Using the representation (6.4) in the decomposition (4.17), the enhanced representation of the second-order wave potential $\varphi_{22}^{(2)}(x,z)$ in the variable bathymetry subdomain $D^{(2)}$ is obtained as follows:

$$\varphi_{22}^{(2)}(x,z) = f_{-2,2}(x)z_{-2}^{(2)}(z;x) + f_{22}^{(2)}(x,z) = \sum_{n=-2}^{\infty} f_{n,2}(x)z_n^{(2)}(z;x), \quad -h_2(x) \leqslant z \leqslant 0, \quad a \leqslant x \leqslant b. \quad (6.5)$$

The above representation, apart from the propagating ($n=0$) and the evanescent ($n \geqslant 1$) modes, involves two additional non-standard terms:

(i) The *free-surface mode* $f_{-2,2}(x)z_{-2}^{(2)}(z;x)$, which has already been defined by (4.17b) to be

$$f_{-2,2}(x) = F_{22}(x), \quad z_{-2}^{(2)}(z;x) = \frac{\cosh[2k_0^{(2)}(x)(z+h_2(x))]}{2k_0^{(2)}(x)\sinh(2k_0^{(2)}(x)h_2(x)) - \mu_2\cosh(2k_0^{(2)}(x)h_2(x))}. \quad (6.6)$$

This extra mode is introduced to ensure the satisfaction of the non-homogeneous free-surface boundary condition of the 2ω problem; see § 4.3. The vertical structure ($z_{-2}^{(2)}(z;x)$) of this mode is a Stokes waveform, locally bound to the linearized propagating mode $\varphi_1(x)Z_1^{(2)}(z;x)$ in the variable bathymetry subdomain $D^{(2)}$. Other choices for $z_{-2}^{(2)}(z;x)$ are also possible, but the one given above seems the most natural and leads to numerically improved matching at the vertical interfaces $x=a$ and $x=b$.

(ii) *The sloping-bottom mode* $f_{-1,2}(x)z_{-1}^{(2)}(z;x)$, with $z_{-1}^{(2)}(z;x) = Z_{-1}^{(2)}(z;x)$, accounting for the satisfaction of the bottom boundary condition on a sloping bottom. The necessity of this term has been thoroughly discussed in AB, where it is shown that the classical representation consisting only of the propagating and the evanescent modes ($f_{n,2}(x)z_n^{(2)}(z;x), n \geqslant 0$) is not consistent with the sloping-bottom boundary condition

and, thus, does not ensure uniform convergence of $\varphi_{22}^{(2)}(x,z)$ and its derivatives up to the bottom boundary $z=-h_2(x)$.

Furthermore, by using (6.6) in the representations (6.4) and (6.5), we easily obtain the following result, connecting the vertical derivative of the second-order wave potential on the bottom $z=-h_2(x)$ with the amplitude of the sloping-bottom mode:

$$\frac{\partial\varphi_{22}^{(2)}(x,z=-h_2(x))}{\partial z}=\frac{\partial f_{22}^{(2)}(x,z=-h_2(x))}{\partial z}=f_{-1,2}(x). \tag{6.7}$$

6.2. *Representation of the steady second-order potential in the variable bathymetry region*

Working similarly we obtain the following local-mode representation of the steady second-order potential $f_{20}^{(2)}(x,z)$:

$$f_{20}^{(2)}(x,z)=f_{-1,0}(x)T_{-1}^{(2)}(z;x)+\sum_{n=0}^{\infty}f_{n,0}(x)T_n^{(2)}(z;x)=\sum_{n=-1}^{\infty}f_{n,0}(x)T_n^{(2)}(z;x),$$
$$-h_2(x)\leqslant z\leqslant 0,\quad a\leqslant x\leqslant b, \tag{6.8}$$

where $f_{n,0}(x)$, $n=-1,0,1,\ldots$, denote the modal amplitudes of the second-order wave potential $f_{20}^{(2)}(x,z)$, and $T_n^{(2)}(z;x)=\cos(n\pi z/h_2(x))$, $n=0,1,2,\ldots$. The additional term $f_{-1,0}(x)T_{-1}^{(2)}(z;x)$, with $T_{-1}^{(2)}(z;x)=Z_{-1}^{(2)}(z;x)$, (6.2*c*), the *sloping-bottom mode*, is the correction term accounting for the exact satisfaction of the boundary condition on a sloping bottom.

Consequently, by using the decomposition (4.19), the enhanced representation of the steady second-order potential $\varphi_{20}^{(2)}(x,z)$ in the variable bathymetry subdomain $D^{(2)}$ is obtained as

$$\varphi_{20}^{(2)}(x,z)=f_{-2,0}(x)T_{-2}^{(2)}(z;x)+f_{20}^{(2)}(x,z)=\sum_{n=-2}^{\infty}f_{n,0}(x)T_n^{(2)}(z;x),$$
$$-h_2(x)\leqslant z\leqslant 0,\quad a\leqslant x\leqslant b. \tag{6.9}$$

Again, this representation, apart from the usual ($n\geqslant 0$) local modes, and the sloping-bottom mode ($n=-1$), involves the *free-surface mode* $f_{-2,0}(x)T_{-2}^{(2)}(z;x)$, where $T_{-2}^{(2)}(z;x)$ denotes its vertical structure, and its amplitude has already been defined by (4.19*a*) to be

$$f_{-2,0}(x)=F_{20}(x). \tag{6.10}$$

This extra mode is introduced to ensure the satisfaction of the non-homogeneous free-surface boundary condition of the steady second-order problem; see § 4.3. We remark that, except for the smoothness requirements concerning $T_{-2}^{(2)}(z;x)$, its vertical shape can be arbitrarily selected, subject to the constraints imposed by the following end-conditions:

$$\frac{\partial T_{-2}^{(2)}(z=0;x)}{\partial z}=1,\quad \frac{\partial T_{-2}^{(2)}(z=-h_2(x);x)}{\partial z}=0. \tag{6.11a,b}$$

Using (6.11*a*) and the definitions of $T_n^{(2)}(z;x)$, $n=-1,0,1,2,\ldots$, in the representation (6.9), we obtain that the vertical derivative of the steady second-order potential on the free surface ($z=0$) is

$$\frac{\partial\varphi_{20}^{(2)}(x,z=0)}{\partial z}=f_{-2,0}(x)=F_{20}(x), \tag{6.12}$$

exactly as required by the non-homogeneous, free-surface boundary condition of the steady second-order problem. Furthermore, using (6.11b) in the representations (6.8) and (6.9), we obtain the following relation connecting the vertical derivative of the steady second-order potential on the sloping bottom ($z = -h_2(x)$) with the amplitude of the (corresponding) sloping-bottom mode:

$$\frac{\partial \varphi_{20}^{(2)}(x, z = -h_2(x))}{\partial z} = \frac{\partial f_{20}^{(2)}(x, z = -h_2(x))}{\partial z} = f_{-1,0}(x), \tag{6.13}$$

which is to be determined, so that the bottom boundary condition

$$f_{-1,0}(x) + \frac{\mathrm{d}h_2(x)}{\mathrm{d}x} \frac{\partial \varphi_{20}^{(2)}(x, z = -h_2(x))}{\partial x} = 0,$$

is satisfied. One possible choice for $T_{-2}^{(2)}(z; x)$, satisfying both smoothness requirements and conditions (6.11a, b), is the function given by (4.19b), which is simply an upside-down form of the sloping-bottom mode, i.e. $T_{-2}^{(2)}(z; x) = -T_{-1}^{(2)}(-z - h_2; x)$.

We are now in a position to give the definition of the admissible function spaces $\boldsymbol{A}_r(D^{(2)})$ for the functions $f_{2r}^{(2)}(x, z)$, $r = 2, 0$, to be used in conjunction with the variational principle of the problems $\mathscr{P}_{T,2r}$, $r = 2, 0$, stated in Theorem B. These function spaces are defined by

$$\boldsymbol{A}_r(D^{(2)}) = \{\psi(x, z) \in \boldsymbol{C}^2(D^{(2)}) \cap \boldsymbol{C}^1(\bar{D}^{(2)}) : \partial\psi/\partial z - \delta_{2r}\mu_2\psi = 0 \text{ on } \partial D_F^{(2)}\}, \quad r = 2, 0,$$

where $\boldsymbol{C}^k(\circ)$ are the usual spaces of functions having continuous derivatives up to order k, and $\bar{D}^{(2)} = D^{(2)} \cup \partial D^{(2)}$. They are more restricted than the ones assumed in formulating Theorem B, since all of its elements satisfy *a priori* the homogeneous, second-order free-surface condition. This more efficient choice for the admissible functions $f_{2r}^{(2)}(x, z)$, $r = 2, 0$, is more accurately restated in the form of the following theorem.

THEOREM C. *The representation theorem*: *Any function* $\psi(x, z) \in \boldsymbol{A}_r(D^{(2)})$ *can be uniquely expanded in a series of the form*

$$r = 2: \quad \psi(x, z) = \sum_{n=-1}^{\infty} \psi_n(x) z_n^{(2)}(z; x), \quad a \leqslant x \leqslant b, \quad -h_2(x) \leqslant z \leqslant 0, \tag{6.14a}$$

$$r = 0: \quad \psi(x, z) = \sum_{n=-1}^{\infty} \psi_n(x) T_n^{(2)}(z; x), \quad a \leqslant x \leqslant b, \quad -h(x) \leqslant z \leqslant 0, \tag{6.14b}$$

where $z_n^{(2)}(z; x)$ *and* $T_n^{(2)}(z; x)$, *have been defined previously. The functions* $\psi_n(x)$ *are appropriate amplitude functions belonging to* $C^2((a, b)) \cap C^1([a, b])$. *The representations* (6.12) *are absolutely and uniformly, along with their termwise derivatives, convergent in the closed domain* $\bar{D}^{(2)} = \{(x, z),\ a \leqslant x \leqslant b,\ -h(x) \leqslant z \leqslant 0\}$.

7. The coupled-mode system of equations for the second-order problems

Let us reconsider the variational principles of the second-order problems, Theorem B, assuming that $f_{2r}^{(2)}(x, z) \in \boldsymbol{A}_r(D^{(2)})$, $r = 2, 0$. Then, by means of the enhanced representations (6.4) and (6.8) (see also Theorem C), the functionals $\mathscr{F}_r(f_{2r}^{(2)}(x, z), \{C_{n,r}^{(1)}\}_{n=0,1,2,\ldots}, \{C_{n,r}^{(3)}\}_{n=0,1,2,\ldots})$, given by (5.2), are transformed to equivalent

functionals of the form

$$\mathscr{F}_r = \mathscr{F}_r\left(\left\{\begin{array}{c} b \\ f_{n,r}(x) \\ a \end{array}\right\}_{n=-1,0,1,2,\ldots}, \{C^{(1)}_{n,r}\}_{n=0,1,2,\ldots}, \{C^{(3)}_{n,r}\}_{n=0,1,2,\ldots}\right), \quad r = 2,0, \tag{7.1}$$

where the sub-a and over-b denote the range of the dummy variable x, according to Volterra's notation. In this way, the degrees of freedom of the system associated with the admissible second-order potentials $f^{(2)}_{2r}(x,z)$, $r = 2,0$, in $D^{(2)}$ (interior points) and $f^{(2)}_{2r}(x,z)$ on $z = -h_2(x)$ (bottom boundary values) are equivalently described by the modal amplitudes $f_{n,r}(x), x \in (a,b)$, $n = -1,0,1,\ldots$, $r = 2,0$. Associated with the vertical interfaces at $x = a$ and at $x = b$ are the degrees of freedom $\{f_{n,r}(a)\}_{n=0,1,\ldots}$ and $\{f_{n,r}(b)\}_{n=0,1,\ldots}$ of the amplitude values at the left-endpoint $x = a$, and at the right-endpoint $x = b$, respectively, as well as the sets of coefficients $\{C^{(1)}_{n,r}, n = 0,1,2,\ldots\}$ and $\{C^{(3)}_{n,r}, n = 0,1,2,\ldots\}$, $r = 2,0$. The amplitudes of the free-surface modes $f_{-2,r}(x)$, $x \in (a,b)$, $r = 2,0$, have been set by (6.6) and (6.10), respectively.

7.1. *Horizontal coupled-mode system of equations*

Taking into account that any admissible function $f^{(2)}_{2r}(x,z)$, $r = 2,0$, satisfies the homogeneous free-surface boundary condition, (5.1*b*), the third integral on the left-hand side of (5.3*b*) can be dropped. Moreover, by assuming that all variations except $\delta f^{(2)}_{2r}(x,z)$ in $D^{(2)} \cup \partial D^{(2)}_{\Pi}$ are zero, the last four integrals of (5.3*b*) can be dropped, giving

$$-\int_{D^{(2)}} (\nabla^2 f^{(2)}_{2r} - g_r)\delta f^{(2)}_{2r}\,\mathrm{d}V + \int_{\partial D^{(2)}_{\Pi}} \left(\frac{\partial f^{(2)}_{2r}}{\partial n^{(2)}} - b_r\right)\delta f^{(2)}_{2r}\,\mathrm{d}S = 0. \tag{7.2}$$

By introducing in the above equation the representations (6.4) and (6.8) for $f^{(2)}_{2r}$, $r = 2,0$, respectively, and their consequence concerning the expressions for $\delta f^{(2)}_{2r}$, and by using (5.4), we obtain the variational equation:

$$\sum_{m=-1}^{\infty} \int_{x=a}^{x=b} \delta f_{m,r}(x) \left[\sum_{n=-1}^{\infty} a_{mn,r}(x)\frac{\mathrm{d}^2 f_{n,r}(x)}{\mathrm{d}x^2} + b_{mn,r}(x)\frac{\mathrm{d}f_{n,r}(x)}{\mathrm{d}x} + c_{mn,r}(x) f_{n,r}(x) - g_{m,r}(x)\right]\mathrm{d}x = 0, \tag{7.3}$$

where

$$g_{m,r}(x) = \begin{cases} -\displaystyle\int_{z=-h_2}^{z=0} \Delta S^{(2)}_{22}(x,z) z^{(2)}_m(z)\,\mathrm{d}z - \frac{\mathrm{d}h_2}{\mathrm{d}x}\frac{\partial S^{(2)}_{22}(x,-h_2)}{\partial x} z^{(2)}_m(-h_2), & r = 2 \\ -\displaystyle\int_{z=-h_2}^{z=0} \Delta S^{(2)}_{20}(x,z) T^{(2)}_m(z)\,\mathrm{d}z - \frac{\mathrm{d}h_2}{\mathrm{d}x}\frac{\partial S^{(2)}_{20}(x,-h_2)}{\partial x} T^{(2)}_m(-h_2), & r = 0. \end{cases} \tag{7.4}$$

The x-dependent coefficients $a_{mn,r}(x)$, $b_{mn,r}(x)$ and $c_{mn,r}(x)$, $r = 2,0$, are given by

$$a_{mn,r}(x) = \int_{z=-h_2(x)}^{z=0} Z_{m,r}(z;x) Z_{n,r}(z;x)\,\mathrm{d}z, \tag{7.5a}$$

$$b_{mn,r}(x) = 2\int_{z=-h_2(x)}^{z=0} Z_{m,r}(z;x)\frac{\partial Z_{n,r}(z;x)}{\partial x}\mathrm{d}z + \frac{\mathrm{d}h_2(x)}{\mathrm{d}x} Z_{m,r}(-h_2(x);x) Z_{n,r}(-h_2(x);x), \tag{7.5b}$$

$$c_{mn,r}(x) = \int_{z=-h_2(x)}^{z=0} Z_{m,r} \frac{\partial^2 Z_{n,r}(z;x)}{\partial x^2}\,\mathrm{d}z + \frac{\mathrm{d}h_2(x)}{\mathrm{d}x} Z_{m,r}(-h_2(x);x) \frac{\partial Z_{n,r}(-h_2(x);x)}{\partial x} + \delta_{-\ln} Z_{m,r}(-h_2(x);x), \quad (7.5c)$$

where δ_{mn} is Kronecker's delta, and

$$Z_{n,r}(z;x) = \begin{cases} z_n^{(2)}(z;x), & r=2, \\ T_n^{(2)}(z;x), & r=0, \end{cases} \qquad n=-1,0,1,2\ldots. \quad (7.5d)$$

Since $\delta f_{m,r}(x)$, $m=-1,0,1,\ldots$ are arbitrary, independent variations, (7.3) is equivalent to the following systems:

$$\sum_{n=-1}^{\infty} a_{mn,r}(x)\frac{\mathrm{d}^2 f_{n,r}(x)}{\mathrm{d}x^2} + b_{mn,r}(x)\frac{\mathrm{d}f_{n,r}(x)}{\mathrm{d}x} + c_{mn,r}(x) f_{n,r}(x) = g_{m,r}(x), \qquad a<x<b, \quad m=-1,0,1,\ldots, \quad (7.6)$$

$r=2,0$, which will be called the *second-order coupled-mode systems of horizontal equations*. The structure of these systems is very similar to the structure of the corresponding system for the linearized potential, (6.3). The coefficients $a_{mn,r}(x)$, $b_{mn,r}(x)$ and $c_{mn,r}(x)$ are all known since they are expressed in terms of the (known) second-order local bases $Z_{n,r}(z;x)$, $r=2,0$. The forcing terms $g_{m,r}(x)$ of the above system are completely defined by (7.4) in terms of the known functions $S_{2r}(x,z)$, which implicitly express the effects of the linearized solution.

7.2. *Boundary conditions for the modal amplitude functions*

Since the system (7.5) is equivalent to (7.2), retaining the former renders the latter an identity. Thus, the variational equation (5.3*b*) can be now simplified to

$$\int_{\partial D_I^{(12)}} \left(\frac{\partial f_{2r}^{(1)}}{\partial n^{(1)}} + \frac{\partial f_{2r}^{(2)}}{\partial n^{(2)}} - \tilde{G}_r^{(12)} \right) \delta f_{2r}^{(2)} \mathrm{d}S + \int_{\partial D_I^{(23)}} \left(\frac{\partial f_{2r}^{(2)}}{\partial n^{(2)}} + \frac{\partial f_{2r}^{(3)}}{\partial n^{(3)}} - \tilde{G}_r^{(23)} \right) \delta f_{2r}^{(2)}\,\mathrm{d}S + \int_{\partial D_I^{(12)}} (f_{2r}^{(2)} - f_{2r}^{(1)} - G_r^{(12)}) \delta \left(\frac{\partial f_{2r}^{(1)}}{\partial n^{(1)}} \right) \mathrm{d}S + \int_{\partial D_I^{(23)}} (f_{2r}^{(2)} - f_{2r}^{(3)} - G_r^{(23)}) \delta \left(\frac{\partial f_{2r}^{(3)}}{\partial n^{(3)}} \right) \mathrm{d}S = 0, \quad r=2,0. \quad (7.7)$$

Similarly to the linearized potential (see AB, § 5), we derive from (7.7) sets of decoupled boundary conditions for each of the modes of the second-order potentials $f_{n,r}$, $n=0,1,2,\ldots$, $r=2,0$, at the ends $x=a$ and $x=b$ of the variable bathymetry region $D^{(2)}$. The final results are summarized in the following theorem:

THEOREM D. *The coupled-mode systems*: *The variational equation* (5.3) *and, thus, the transmission problems* $\mathscr{P}_{T,2r}$, $r=2,0$, *are equivalent to the inhomogeneous system of second-order differential equations* (7.6), *supplemented by the following boundary conditions*:

$$f_{-1,r}(a) = \frac{\mathrm{d}f_{-1,r}(a)}{\mathrm{d}x} = 0, \quad f_{-1,r}(b) = \frac{\mathrm{d}f_{-1,r}(b)}{\mathrm{d}x} = 0, \quad (7.8a)$$

$$\left.\begin{aligned} \delta_{2r}\frac{\mathrm{d}f_{0,r}(a)}{\mathrm{d}x} + \chi_{0,r}(a)f_{0,r}(a) &= G_{0,r}(a), \\ \frac{\mathrm{d}f_{0,r}(b)}{\mathrm{d}x} - \chi_{0,r}(b)\left(\delta_{2r}f_{0,r}(b) + \delta_{0,r}\frac{\mathrm{d}f_{0,r}(a)}{\mathrm{d}x}\right) &= G_{0,r}(b), \end{aligned}\right\} \tag{7.8b}$$

$$\frac{\mathrm{d}f_{n,r}(a)}{\mathrm{d}x} - \chi_{n,r}(a)f_{n,r}(a) = G_{n,r}(a), \quad \frac{\mathrm{d}f_{n,r}(b)}{\mathrm{d}x} + \chi_{n,r}(b)f_{n,r}(b) = G_{n,r}(b), \quad n = 1, 2, \ldots. \tag{7.8c}$$

The coefficients $\chi_{n,r}$, and the forcing terms $G_{n,r}$, $n = 0, 1, 2, \ldots$, $r = 2, 0$, appearing in the boundary conditions (7.8), are given in Appendix B. Note that conditions (7.8*a*), concerning the sloping-bottom modes $f_{-1,r}(x)$, are not derived from the variational equation (7.7). These conditions are derived using (6.7) and (6.13) and the bottom boundary conditions of the second-order problems, requiring $\partial\varphi_{2r}^{(2)}(x = a, x = -h_1)/\partial z = 0$ and $\partial\varphi_{2r}^{(2)}(x = b, x = -h_3)/\partial z = 0$, in conjunction with the smoothness assumptions concerning the depth function $h(x)$.

The coefficients Λ_R, $\Lambda_n^{(1)}$, Λ_T, $\Lambda_n^{(3)}$ and $\Gamma_n^{(1)}$, $\Gamma_n^{(3)}$, $n = 0, 1, 2, \ldots$, of the representation of the second-order wave potentials in the two half-strips are then obtained by means of the matching conditions (5.1*d*, *e*) and (5.1*f*, *g*) and are listed in Appendix C.

In contrast to the coupled-mode system for the linearized problem, (6.3), where the forcing of the system, due solely to the incident wave, appears only in the boundary condition for the propagating mode at $x = a$ (see AB, § 5), the forcing of the second-order coupled mode systems comes both from the right-hand side of the differential equations (the terms $g_{m,r}(x)$, defined by (7.4)), and from the right-hand side of the boundary conditions (the terms $G_{n,r}(a)$ and $G_{n,r}(b)$ in (7.8)).

In concluding this section, it is worth pointing out that, under the smoothness assumptions for the depth function $h(x)$, the coefficients $a_{mn,r}(x)$, $b_{mn,r}(x)$ and $c_{mn,r}(x)$, $r = 2, 0$, of the second-order coupled-mode systems are continuous functions of x and can be calculated *a priori* in terms of the known local vertical bases. Furthermore, discontinuities of the depth function $h(x)$, or of its derivative, can also be treated by introducing appropriate domain decomposition with matching boundaries at the points of discontinuities, see e.g. Massel (1983) for the treatment of the 2ω problem in the case of an infinite underwater step. Finally, it should be remarked here that the present theory can be extended to treat the case of obliquely incident waves over variable bathymetry.

8. Numerical results and discussion

The coupled-mode systems (7.6), (7.8) for the two second-order problems ($r = 2, 0$) have been solved by means of a second-order finite-difference discretization scheme. The method of solution is similar with the one presented in AB, § 6, in conjunction with the linearized problem.

In this section, numerical results are first presented for the case of a smooth, but steep, underwater shoal, selected as an example in order to illustrate various aspects of the second-order coupled-mode theory in variable bathymetry regions. Then, the present method is validated against (i) experimental data for the case of a bar with rounded corners (Rey *et al.* 1992), (ii) other second-order models and experimental data for the case of a submerged trapezoidal bar (Ohyama *et al.* 1995*b*), and (iii) nonlinear numerical solutions (Ohyama & Nadaoka 1994), for the case of an underwater step.

8.1. *Discrete approximation of the coupled-mode system of equations*

First the series (6.4) and (6.8) are truncated to a finite number of terms (modes), retaining N_e evanescent modes along with the propagating ($n = 0$), the sloping bottom ($n = -1$) and the free-surface ($n = -2$) modes. The last have been defined by (6.6) and (6.10), for $r = 2$ and $r = 0$, respectively, in terms of the linearized potential.

The discrete scheme is constructed by using central, second-order, finite differences for approximating the first and second derivatives of the coupled-mode systems (7.6), in $[a, b]$. Second-order discrete boundary conditions are obtained by combining (7.8) and (7.6) at the ends $x = a$, $x = b$, and then using central differences to approximate derivatives.

It is well known that the spatial degree of approximation of the discrete system, specified by the number N of segments subdividing the interval $[a, b]$, is strongly dependent on the local variation of the wave potentials, which, in the case of the 2ω problem, is controlled by the local wavelength. A standard rule is to use at least 10 grid points per (local) wavelength. Taking into account that the second-order wave potential varies twice as rapidly as the first-order one, the previous requirement may lead to a significant increase of the dimension of the discrete system, if the number of modes $N_m = N_e + 2$, required for the convergence of the numerical solution is not small. This situation becomes more problematic as the frequency and/or the bottom variation length $(b - a)$ increase. Thus, it is important to keep the number of modes N_m required for the numerical convergence of the solution as small as possible, without sacrificing the quality of the results.

The number N_m is essentially dependent on the local bottom slope and curvature. A good deal of experience concerning the numerical behaviour of the modal series has been acquired in connection with the linearized problem; see AB, § 6, and its extension to three dimensions (Athanassoulis *et al.* 2000). In the case of a slowly varying bathymetry, representation (6.1), associated with the linearized potential, can be drastically simplified by dropping all evanescent modes φ_n, $n = 1, 2, 3, \ldots$, and the sloping-bottom mode φ_{-1}, leading to the *modified mild-slope* model (Massel 1993; Chamberlain & Porter 1995). As the bottom surface becomes locally more steep, the inclusion of evanescent modes in the representation is inevitable. However, the inclusion of the sloping-bottom mode greatly alleviates this situation, by increasing the rate of decay of the modal-amplitude functions φ_n from $O(n^{-2})$, when φ_{-1} is not included, to $O(n^{-4})$, when φ_{-1} is taken into account. In what follows, by means of a simple numerical example, we shall demonstrate that the fast decay property still holds for the representations (6.4) and (6.8) of the second-order potentials in the variable bathymetry region. This renders the present model a valuable tool for the study of weakly nonlinear waves over uneven bottom profiles with steep slopes.

8.2. *Illustration of various features of the second-order coupled-mode theory through a numerical case study*

As a first example, let us consider the following (monotocically varying) depth function:

$$h(x) = \begin{cases} h_1 = 6\,\mathrm{m}, & x < a = 10\,\mathrm{m}, \\ h_2(x) = \dfrac{h_1 + h_3}{2} - \dfrac{h_1 - h_3}{2} \tanh\left(3\pi\left(\dfrac{x-a}{b-a} - \dfrac{1}{2}\right)\right), & a < x < b, \\ h_3 = 2\,\mathrm{m}, & x > b = 30\,\mathrm{m}, \end{cases} \tag{8.1}$$

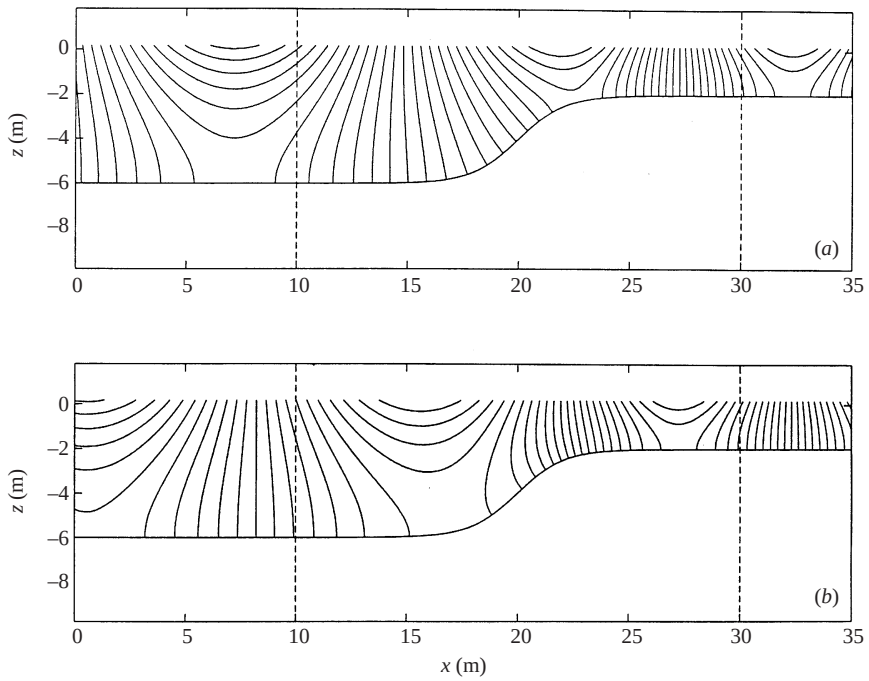

FIGURE 4. (*a*) Real and (*b*) imaginary first-order wave field $\varphi_1(x, z)$ in the case of the smooth but steep shoal, defined by (8.1). Incident wave conditions: $H = 0.2\,\text{m}$, $\omega = 1.3\,\text{rad}\,\text{s}^{-1}$. The maximum bottom slope is $s_{max} = 94\%$, approximately in the middle of the variable bathymetry region $D^{(2)}$, indicated by vertical dashed lines.

which represents a smooth, but locally very steep, underwater shoal, joining a water region of 6 m depth with a shallow water region of 2 m depth. This bathymetry has also been studied in AB in connection with the application of the coupled-mode technique to the linearized problem.

The maximum bottom slope of the underwater shoal (8.1) is $s_{max} = 0.94$ and the mean bottom slope $s_{mean} = 0.2$. A sketch of the bottom geometry is shown in figure 4. Numerical results for this bottom geometry, and for an incident wave of angular frequency $\omega = 1.3\,\text{rad}\,\text{s}^{-1}$, and wave height $H = 0.2\,\text{m}$, are presented and discussed in figures 4 to 10 for this geometry. The incident wave has been assumed to be purely monochromatic, i.e. $A_0 = 0$.

In the case examined both shallowness ratios $h_1/\lambda_1 = 0.19$ and $h_3/\lambda_3 = 0.1$ fall well outside the limits of the deep or the shallow water theory. The Ursell parameter $U = (H/h)(\lambda/h)^2$ varies from $U_1 = 0.87$ to $U_3 = 11.1$, on moving from the region of incidence to the region of transmission. Thus, the pair $(U, H/\lambda)$ falls well within the regime of Stokes theory, bounded by $U < 8\pi^2$ and $H/\lambda < 0.14\tanh(2\pi h/\lambda)$; see e.g. Massel (1989). The modulus of the reflection coefficient has been calculated to be $|A_R| = 0.116$ and the modulus of the transmission coefficient $|A_T| = 1.096$, which are very close to the corresponding values for the abrupt underwater step shown in figure 2.

In figure 4 the equipotential lines of the linearized wave potential $\varphi(x, z)$ (real and imaginary parts) in the variable bathymetry subdomain $D^{(2)}$ have been plotted. Numerical results shown have been obtained by subdividing the range $b - a = 20\,\text{m}$ into $N = 100$ segments, and by retaining 6 evanescent modes ($N_e = 6$) in the

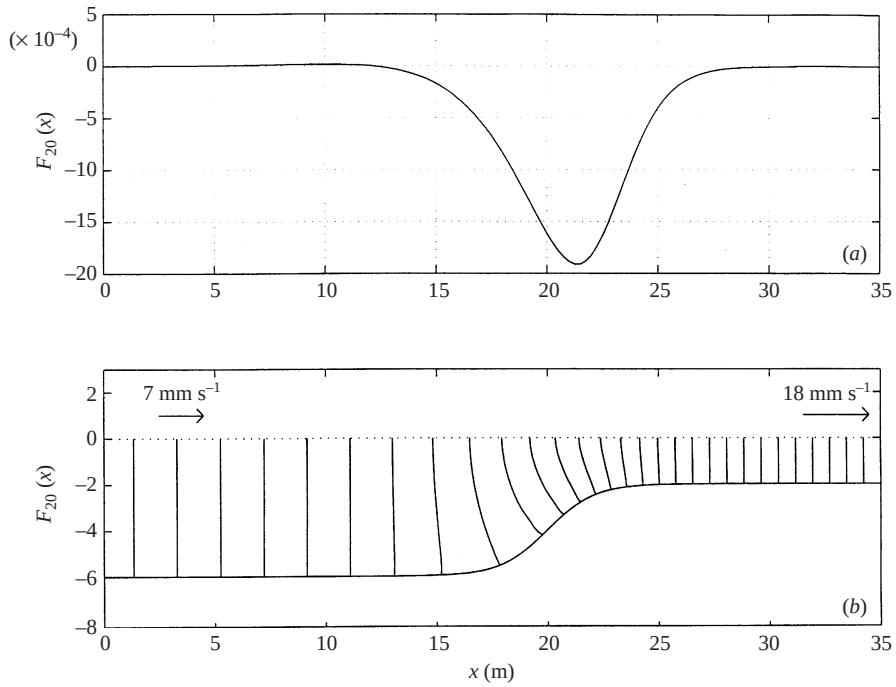

FIGURE 5. (*a*) Forcing $F_{20}(x)$ of the steady second-order problem, for the same environment and wave conditions as in figure 4. (*b*) Solution of the steady second-order problem $\varphi_{20}(x, z)$, as calculated by the present method.

representation, which was found to be enough for the convergence of the numerical solution. In this figure, the fulfilment of the bottom boundary condition is clearly seen, which is equivalent to the normal intersection of the equipotential lines and the bottom profile. We can observe the fine matching, at $x = a$ and at $x = b$, between the representations of the wave potential in the three subdomains.

Based on the calculated linearized wave potential, the forcing of the free-surface boundary condition of the steady second-order problem $F_{20}(x)$ is plotted in figure 5(*a*). Clearly, $F_{20}(x)$ exhibits a very fast (exponential) decay moving away from the variable bathymetry region, as already discussed at the end of § 4.2. Thus, the forcing of the steady second-order problem is essentially concentrated over the variable bathymetry region, inside the interval $[a, b]$, and is maximized along with the bottom slope.

The steady second-order wave field $\varphi_{20}(x, z)$ (induced current) is shown in figure 5(*b*), by equipotential lines. Again, the equipotential lines intersect the bottom profile perpendicularly, as they should. In the case examined, the steady field generates a slow current in the same direction as the wave, and with velocities ranging from $u_{20}^{-\infty} = 6.9\,\mathrm{mm\,s^{-1}}$, in the deep-water region, to $u_{20}^{+\infty} = 17.6\,\mathrm{mm\,s^{-1}}$, in the shallow-water region. Thus, the mass imbalance coefficient generated by the steady current is

$$\delta M_{av}^{C} = \frac{M_{av}^{C}(+\infty) - M_{av}^{C}(-\infty)}{\rho\omega H^2} = \frac{\rho(u_{20}^{+\infty} h_3 - u_{20}^{-\infty} h_1)}{\rho\omega H^2} = -0.125. \qquad (8.2a)$$

On the other hand, by using (3.8*b*) and the calculated values of the reflection and transmission coefficients of the linearized problem, the wave-generated mass flux

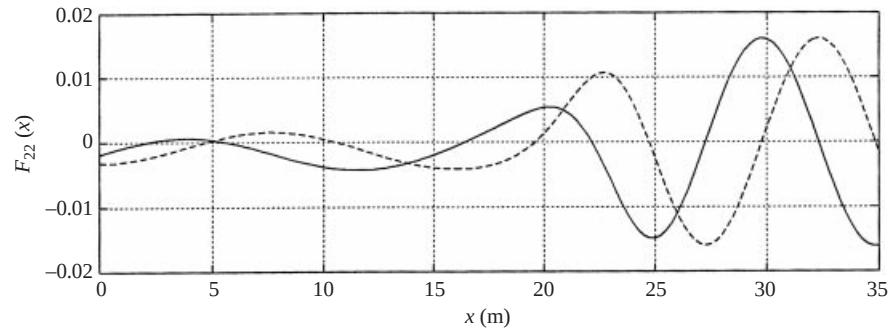

FIGURE 6. Real (solid line) and imaginary (dashed line) parts of the forcing $F_{22}(x)$ of the second-order wave potential, for the same environment and wave conditions as in figure 4.

imbalance is

$$\delta M_{av}^{W} = \frac{M_{av}^{W}(+\infty) - M_{av}^{W}(-\infty)}{\rho\omega H^2} = \frac{g}{8\omega^2}(k_0^{(3)}|A_T|^2 - k_0^{(1)}(1 - |A_R|^2)) = 0.125, \quad (8.2b)$$

which exactly balances the current-generated flux. Note that the calculated value of $\delta M_{av}^{W} = 0.125$, for $\omega = 1.3\,\mathrm{rad\,s^{-1}}$, is very close to the corresponding value obtained in the case of the underwater step with the same depths at infinity, plotted in figure 2.

In figure 6 the real and imaginary parts of the forcing $F_{22}(x)$ of the second-order wave problem are plotted, as calculated by means of the linearized wave potential, (2.9). Unlike the forcing $F_{20}(x)$ of the steady problem, which decays exponentially away from the variable bathymetry region, $F_{22}(x)$ extents all along the real axis from $-\infty$ to ∞. It is clearly seen in figure 6 that $F_{22}(x)$ increases substantially as we move from the region of incidence (deeper water) to the region of transmission (shallower water). This observation is indicative of the second-harmonic generation which is expected to occur as the shallow end of the variable bathymetry is approached. The unsteady second-order wave field $\varphi_{22}(x, z)$, as calculated by the present method, is plotted in figure 7, by equipotential lines. The fulfilment of the bottom boundary condition and the smooth matching of the second-order representations in the three subdomains, at $x = a$ and at $x = b$, are again evident. The free-surface elevation associated with the first and the second harmonics is presented in figure 8. The linearized free-surface elevation $\varepsilon\eta_1(x) = \frac{1}{2}H\varphi_1(x)$ (see (2.7)) is the dominant part. The second-harmonic generation, represented by the wave elevation $\varepsilon^2\eta_{22}(x)$, becomes appreciable as the shallow end of the smooth shoal is approached. In this area the amplitude of the second harmonic reaches about 20% of the amplitude of the first harmonic. Under the wave conditions examined, the contribution of $\varepsilon^2\eta_{20}(x)$ (i.e. the mean sea level set-down) is negligible.

In figure 9 the moduli of the modal-amplitude functions, i.e. the quantities $|\varphi_n(x)|$, and $|f_{n,r}(x)|$, $r = 2, 0$, in $a \leqslant x \leqslant b$, are plotted, as obtained by the present method. The horizontal axis in figure 9 is a multiple replica of the interval $[a, b]$, i.e. a sequence of repeated intervals $[a, b]$, each associated with a mode and named after the mode number. In the nth replica of $[a, b]$ the amplitudes $|\varphi_n(x)|$ and $|f_{n,r}(x)|$, $r = 2, 0$, of the nth mode are plotted using solid, dashed and dash-dotted lines, respectively. Also, the curve $0.1n^{-4}$ is drawn, bounding the maxima of the amplitudes of all modal functions, both of the linearized and of the second-order potentials. On the basis of these (and many other similar) results, we can conjecture that the decay of the modal amplitudes is $O(n^{-4})$, which is sufficient to ensure the uniform convergence

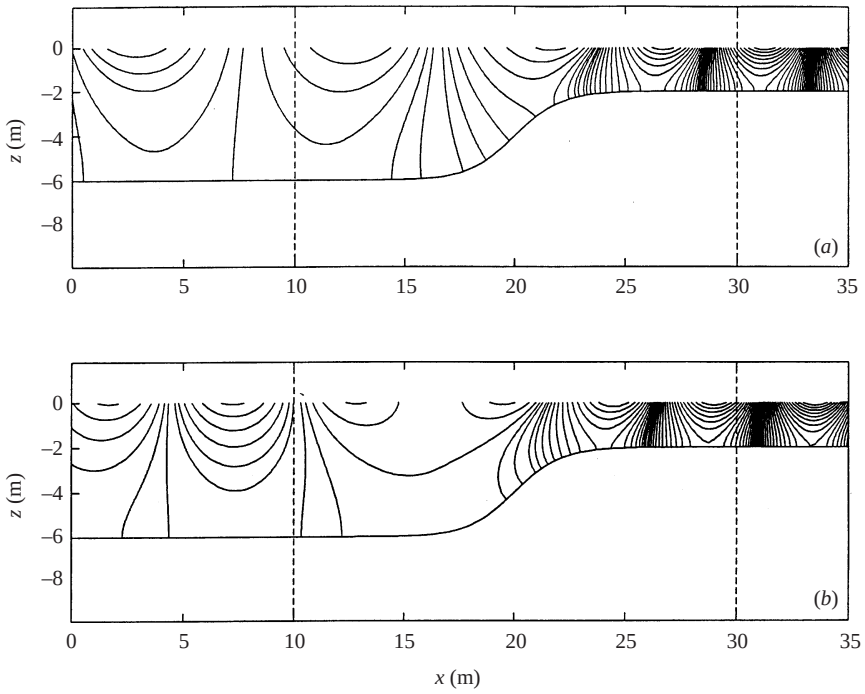

FIGURE 7. Solution of the second-order wave problem $\varphi_{22}(x, z)$, for the same environment and wave conditions as in figure 4, as calculated by the present method: (*a*) real part, (*b*) imaginary part. The vertical dashed lines indicate the limits of the variable bathymetry domain.

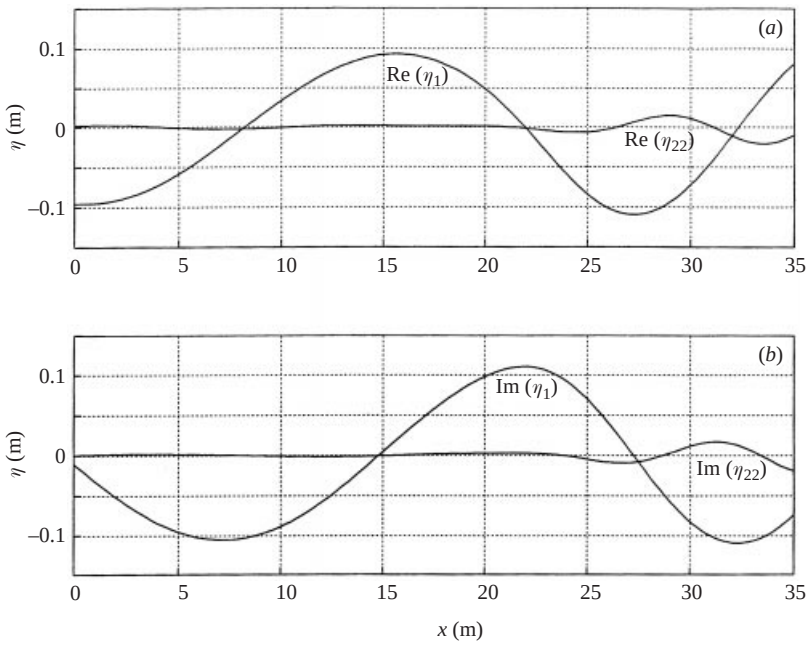

FIGURE 8. First and second harmonics of the free-surface elevation, for tha same environment and wave conditions as in figure 4: (*a*) real part, (*b*) imaginary part.

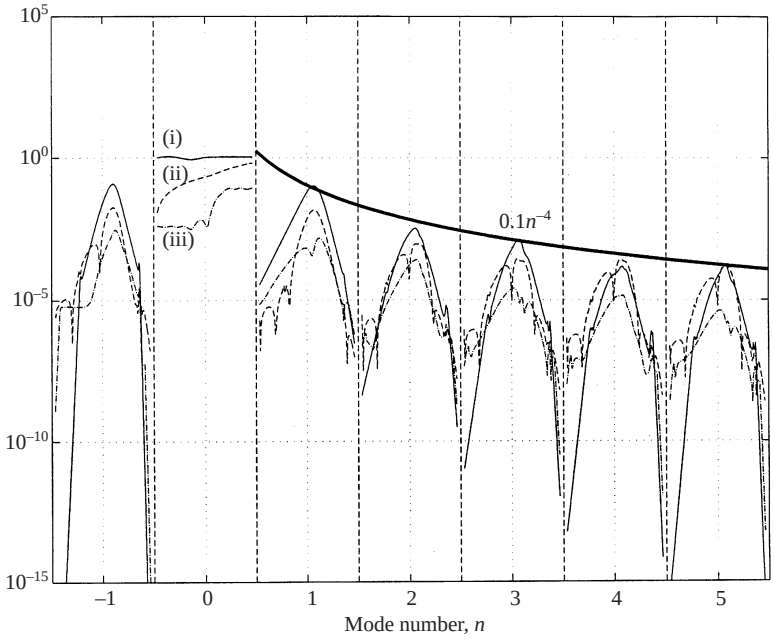

FIGURE 9. Moduli of the modal-amplitude functions of first- and second-order potentials vs. $x \in [a, b]$ in the variable bathymetry region, for various modes $n = -1, 0, 1, 2, \ldots$: (i) amplitudes of the linearized problem $|\varphi_n(x)|$ (solid line), (ii) amplitudes of the steady second-order problem $|f_{n,0}(x)|$ (dashed line), (iii) amplitudes of the unsteady second-order problem $|f_{n,2}(x)|$ (dash-dotted line). Environment and wave conditions as in figure 4. The curve $0.1n^{-4}$, shown by a thick solid line, bounds the maxima of the modal amplitudes of all potentials.

(up to and including the boundaries) of the corresponding local-mode series and their derivatives. Note that the exact fulfilment of the bottom boundary condition, illustrated for the linearized and the second-order potentials in figures 4, 5(*b*) and 7, respectively, is due to the above fast rate of decay of the modal amplitude functions.

In figure 9 discontinuities seem to appear, particularly in the distribution of the $n = -1$ (sloping-bottom) mode, evident for the linearized and the second-order potentials and more sharp at the point corresponding to the horizontal position $x = 30\,\mathrm{m}$ (shallower end of variable bathymetry region). These discontinuities, magnified by the logarithmic vertical scale used in the plot, are not important. They are due to the very small disturbances of the smoothness of the depth function, as defined by (8.1) for the bathymetry considered. In fact, due to the asymptotic behaviour of tanh for large arguments, at $x = a = 10\,\mathrm{m}$ the depth is $h(x = 10\,\mathrm{m}) = 5.997\,\mathrm{m}$, instead of $h_1 = 6\,\mathrm{m}$, and at $x = b = 30\,\mathrm{m}$, $h(x = 30\,\mathrm{m}) = 2.003\,\mathrm{m}$, instead of $h_3 = 2\,\mathrm{m}$. If we move the matching boundaries further to the left and to the right, these discontinuities completely disappear, leaving the significant part of the distributions of the modal amplitude functions intact.

In figure 10(*a*) the variation of the first-order reflection and transmission coefficients $|A_R|$, $|A_T|$, and the associated second-order net mass flux M, are presented in the whole frequency range, from globally shallow-water wave conditions ($\omega = 0.5\,\mathrm{rad\,s^{-1}}$) to globally deep-water conditions ($\omega = 4\,\mathrm{rad\,s^{-1}}$). These coefficients are almost the same as the ones corresponding to the abrupt underwater step with the same depths at infinity (shown in figure 2). Thus, the wave-generated mass imbalance δM_{av}^{W}, (3.8*b*), is very close to the one plotted in figure 2, and it is not given here. Instead, in

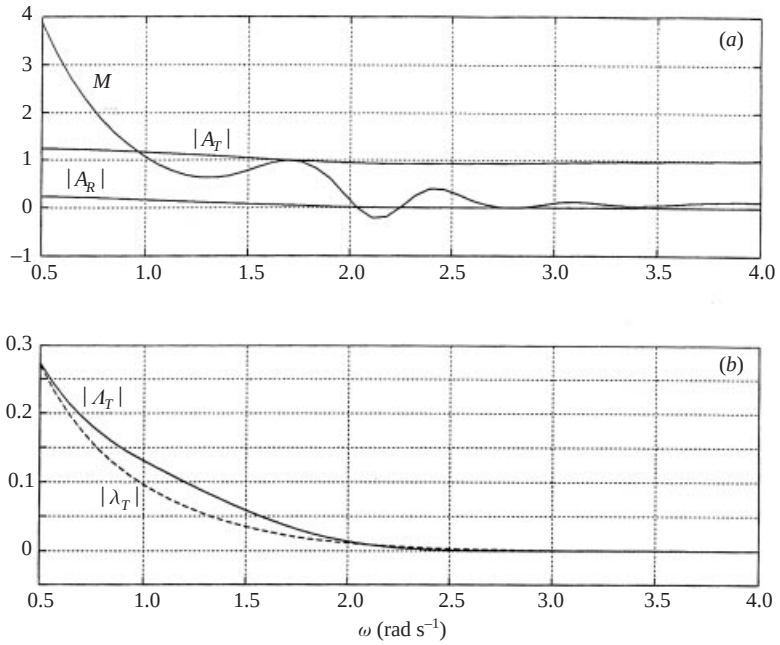

FIGURE 10. (*a*) Moduli of first-order reflection ($|A_R|$) and transmission ($|A_T|$) coefficients, and net mass flux (M) coefficient vs. frequency ω, for the smooth shoaling (8.1). (*b*) Moduli of the second-order transmission coefficients, associated with the free ($|\Lambda_T|$, solid line) and the bound ($|\lambda_T|$, dashed line) second-order waves, respectively.

figure 10(*a*), the net (from the combination of wave and current) mass flux coefficient is presented, defined by

$$M = \frac{M_{av}^W + M_{av}^C}{\rho\omega H^2}, \tag{8.3}$$

which, as anticipated by Theorem A, is constant (x-independent), for a given frequency. We can see from this figure that, the net mass flux can be positive or negative, depending on the frequency of the incident wave, and attains higher values at low frequencies. In the high-frequency limit the net mass flux tends to a definite value ($M \to 1/8$), since the linearized wave passes the step without reflection ($|A_R| \to 0$, $|A_T| \to 1$), and, thus, wave mass flux imbalance is not generated ($\delta M_{av}^W \to 0$). Indeed, in this case, the forcing of the steady second-order problem and the corresponding current flux tend to zero ($F_{20} \to 0, M_{av}^C \to 0$), and thus (cf. (2.2*c*))

$$M = M_{av}^W/\rho\omega H^2 = \tfrac{1}{8}\tanh(kh) \to \tfrac{1}{8}. \tag{8.4}$$

This value agrees quite well with our numerical predictions at $\omega = 4\,\mathrm{rad\,s^{-1}}$ (globally deep-water conditions).

The second-order transmission coefficients $|\lambda_T|$ and $|\Lambda_T|$, associated with the Stokes bound wave and free wave, respectively, are presented in figure 10(*b*) versus frequency. (The corresponding reflection coefficients $|\lambda_R|$ and $|\Lambda_R|$ are negligible and are not plotted.) The coefficients $|\lambda_T|$, $|\Lambda_T|$, which represent the effect of second-harmonic generation in the shallow water region, are monotonically decreasing with frequency. For shallow-water conditions ($\omega \to 0.5\,\mathrm{rad\,s^{-1}}$, for this environment), the bound and free second harmonics in $D^{(3)}$ become comparable in magnitude with the first harmonic

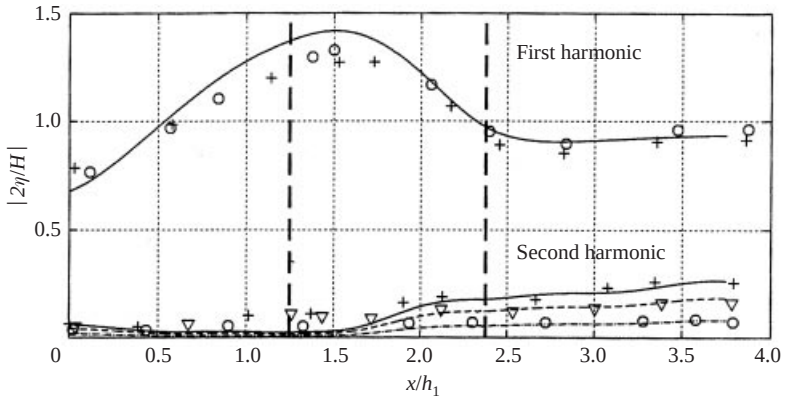

FIGURE 11. Comparison of the present theory (lines) with experimental results (symbols) (Rey *et al.* 1992), in the case of a rounded-corner bar of shoaling ratio 0.375. Incident wave frequency $\omega^2 h_1/g = 0.78$. Incident wave height $H/h_1 = 0.02$ (dash-dotted line vs. circles), 0.045 (dashed line vs. triangles), 0.07 (solid line vs. crosses). The position of the bar is shown by vertical dashed lines.

(about 25% of the latter). The same effect has been also reported by Massel (1983, figures 5, 6) in the case of an abrupt underwater step.

8.3. *Validation against experimental data and comparison with nonlinear numerical solutions*

Experimental results focusing on the second-order features of waver waves propagating over generally shaped, non-mildly sloped, smooth bottom profiles at intermediate-water-depth conditions are not available, at least to the authors' knowledge (although the situation does not seem to be unnatural or exceptional in practice). On the other hand, various experimental studies have been published concerning submerged bars or underwater steps. Among them, the extensive experimental results of Rey *et al.* (1992), concerning the propagation of waves over a single submerged impermeable bar (with sharp and also) with rounded corners, contains a great deal of information about second-harmonic generation and, thus, can be used for validation of the present theory (although appropriate experimental results for a smoother profile would be even better and are strongly desirable).

A comparison of results obtained by the present theory with experimental results from Rey *et al.* (1992, figure 14), is presented in figure 11. The experimental set-up considered refers to the case of a rounded-corner bar having a shoaling ratio $h_{min}/h_1 = 0.375$ and a non-dimensional bar length $L/h_1 = 1.125$, at an intermediate (non-dimensional) frequency $\omega^2 h_1/g = 0.78$. For this configuration, the first and the second harmonics (called in Rey *et al.* fundamental and first harmonics, respectively) of the wave amplitude were measured in the vicinity of the bar, for three values of incident wave height $H/h_1 = 0.02, 0.045, 0.07$. This example was selected for validation purposes, since all the above-stated conditions of the experiment are within the regime of weakly nonlinear water waves in intermediate water depth.

In order to treat the geometry of the vertical walls of the rounded-corner bar by the present theory, the bar has been smoothly approximated by using the tanh form (8.1), with parameters leading to large maximum bottom slope ($s_{max} \gg 1$) at the position of the vertical walls. The results of the present theory, for the three values of the incident wave height $H/h_1 = 0.02, 0.045, 0.07$, are shown in figure 11 by dotted, dashed and solid lines, respectively. Experimental results for the three different wave

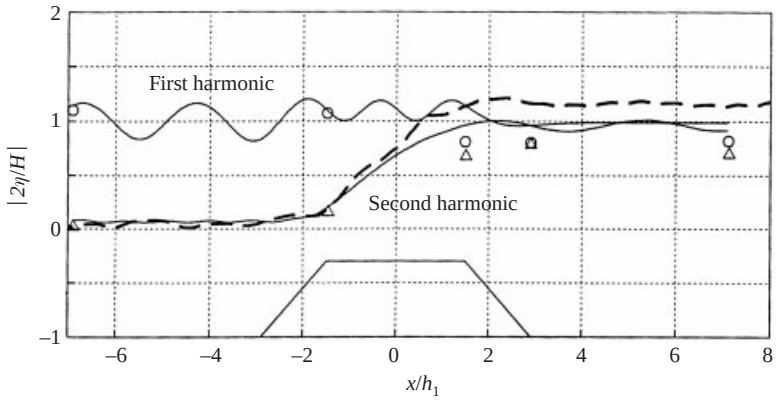

FIGURE 12. Comparison of the present theory (solid lines) vs. second-order numerical solution (Kioka & Ishida 1993, shown by the thick dashed line) and experimental results (Ohyama *et al.* 1995*b*, shown by circles and triangles), in the case of a trapezoidal submerged bar with shoaling ratio 0.3. Wave conditions: $\omega^2 h_1/g = 1.11$, $H/h_1 = 0.1$. The position of the bar is shown in the lower part of the figure.

heights are indicated in figure 11 by circles, triangles and crosses, respectively. The location of the bar is depicted by thick, vertical dashed lines. For both the first and the second harmonics, our numerical predictions agree quite well with experimental data, resolving both the phenomenon of second-harmonic generation (beginning at the face of the bar and continuing up to a distance equal to the bar length after its rear end), and the nonlinearity (increase of the normalized amplitude of the second harmonic with the incident wave amplitude).

As another example, in figure 12 we present a comparison with other second-order model results (Kioka & Ishida 1993, referred to herein as KI) and experimental results from Ohyama *et al.* (1995*b*, Case 2). The experimental set-up considered refers to the case of a trapezoidal submerged bar having a shoaling ratio $h_{min}/h_1 = 0.3$. The bottom slope at the sides of the trapezoidal bar is 50%. The case selected for comparison is characterized by a non-dimensional frequency $\omega^2 h_1/g = 1.11$, and an incident wave height $H/h_1 = 0.1$, leading to a generation of small third and higher harmonics (less than 30% of the basic harmonic). The results of the present theory concerning the first and the second harmonics are shown in figure 12 by solid lines. Results of the KI model are shown by a thick dashed line. (Only the second harmonic is plotted, since the first harmonic practically coincides with our results.) Experimental results are shown by circles (first harmonic) and triangles (second harmonic), respectively.

In this case, the KI model, which is based on an boundary integral equation formulation of the second-order problem, has been criticized as markedly overestimating the second harmonic, in comparison with the fully nonlinear and the Boussinesq models, in the trailing edge of the shelf, Ohyama *et al.* (1995*b*, figure 7). However, as is evident from figure 12, the present second-order model improves this situation.

As a final example, serving both for validation and clarification of the limitations of our approach, we present and discuss a comparison with results of Ohyama & Nadaoka (1994, referred to herein as ON), obtained by means of numerical solution of the fully nonlinear water wave equations, for an infinite underwater step. The case selected for comparison (figure 4 of ON) is characterized by a shoaling ratio $h_3/h_1 = 0.4$, and a non-dimensional frequency $\omega^2 h_1/g = 0.8$. As before, wave conditions and water depths are within the regime of weakly nonlinear wave theory

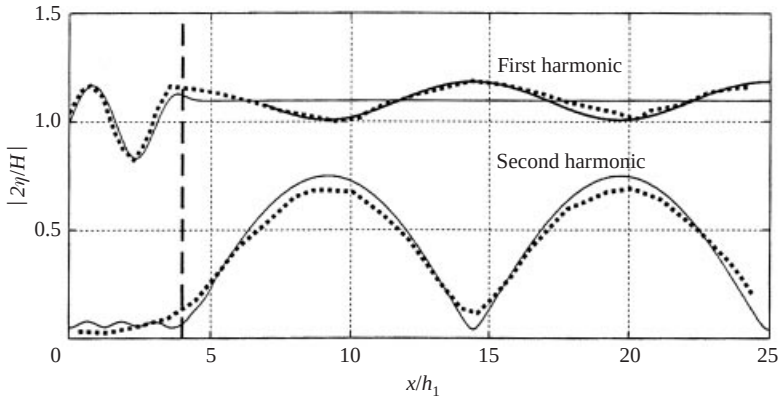

FIGURE 13. Comparison of the present theory (solid lines) with fully nonlinear numerical solution (Ohyama & Nadaoka 1994, shown by dots), in the case of a stepped bottom with shoaling ratio $h_3/h_1 = 0.4$. Wave conditions: $\omega^2 h_1/g = 0.8$, $H/h_1 = 0.1$. The position of the step is shown by a thick vertical dashed line. The result of the bichromatic interaction between the transmitted first and second harmonics, as calculated by the present method, in the transmission region (shallower water depth) is also plotted using a thick line.

in intermediate water depth. Again, to treat the vertical wall of the underwater step, a smooth but steep bottom profile has been used, by appropriately tuning the tanh form (8.1). The first and second harmonics of free-surface elevation, calculated by means of the present method, are plotted in figure 13 by solid lines. The corresponding numerical nonlinear results for the stepped bottom are shown by a thick-dotted line (as digitized from figure 4 of ON). The position of the step is indicated by a thick vertical dashed line. As we can see in figure 13, the present method resolves well the effects of weak nonlinearity. The second harmonic exhibits a modulation length equal to $2\pi/(\kappa_0^{(3)} - 2k_0^{(3)}) = 10.47\,\mathrm{m}$, which is due to the interaction of the second-order bound and free waves in the transmission region, and agrees well with the nonlinear numerical solution.

In this case of moderate shoaling ratio ($h_3/h_1 = 0.4$), our second-order model slightly overestimates the amplitude of the second harmonic in the transmission region, in comparison with the fully nonlinear numerical solution of ON. However, the variation of the amplitude of the first harmonic, which is observed in the numerical nonlinear solution (and also in similar experiments by Bendykowska & Massel 1984) is not directly reproduced by our results. This variation has been recognized by Massel (1983, 1989) and Goda (1997) as a result of non-resonant interaction between the first harmonic $(k_0^{(3)}, \omega)$ and the free second harmonic $(\kappa_0^{(3)}, 2\omega)$, in the transmission region. Applying this interpretation, we also are able to predict this phenomenon quite well, by considering the bichromatic interaction between $(k_0^{(3)}, \omega)$ and $(\kappa_0^{(3)}, 2\omega)$ in constant depth (i.e. in $D^{(3)}$). This interaction generates an additional first harmonic which, when combined with a linearized transmitted wave, produces the spatial variation of the amplitude of the first harmonic, plotted in figure 13 by a thick line. This result, agrees well with the nonlinear numerical solution (ON, figure 4).

As the shoaling ratio h_3/h_1 further decreases, the nonlinearity generated in the shallower water region becomes continuously stronger. From numerical experimentation by ON, (figure 5), in the case of the abrupt step, we know, for example, that for $h_3/h_1 = 0.3$, the second harmonic generated becomes of the order of the first one, and a large amount of energy is transferred to the third harmonic, which can no longer

be neglected. In this case, the present model, being unable to treat the energy transfer to higher harmonics, results in a significant overestimation of the second-harmonic amplitude generated, in comparison with the nonlinear numerical solution of ON. Although the present weakly nonlinear model does not break down for this shoaling ratio (and even smaller values of h_3/h_1), the above situation provides us with an indication of the limits of its reliability.

9. Conclusions and implications for simulation of wave–wave interactions

In the present work the second-order Stokes theory has been extended to the case of a generally shaped bottom profile connecting two half-strips of constant (but possibly different) depths. Thus, a method for generalizing the Stokes hierarchy of second- and higher-order wave theories is initiated, without the assumption of spatial periodicity. The first- and second-order problems have been equivalently reformulated as coupled-mode systems of differential equations in the propagation space (horizontal plane). Apart from the Stokes small-amplitude expansibility assumption, no additional asymptotic assumptions have been introduced, e.g. bottom slope and curvature may be arbitrary, provided that the resulting wave dynamics is Stokes-compatible. Accordingly, the present theory, being valid within the Stokes regime, permits the study of various wave phenomena (propagation, reflection, diffraction) arising from the interaction of weakly nonlinear waves with a general bottom topography, in intermediate water depth. An interesting phenomenon, that is also very naturally resolved by the present theory, is the net mass flux induced by the limiting depth variation $|h_3 - h_1|$, which is consistently calculated by means of the steady second-order potential.

An important technical feature of the present approach is the introduction of two additional modes: one treating the second-order free-surface forcing, and a second one describing the influence of the bottom topography (in general, not mildly sloped and/or strongly oscillating). It turns out that the presence of the slopping-bottom mode in the series representations of the first- and second-order potentials ensures, apart from consistency (see AB, §4), a substantial acceleration of convergence of the modal series, making possible to restrict ourselves to a few (5–7) modes.

The present method has been validated against experimental results and fully nonlinear numerical solutions. It has been found that it correctly predicts the second-order harmonic generation, the amplitude nonlinearity, and the amplitude variation due to non-resonant first-second harmonic interaction. Also, the limitations of applicability of the present model, in connection with the effects of higher harmonic generation due to increased shoaling, have been indicated. Other features worth noticing, including possible extensions of the present theory, are the following: (i) it effectively treats the non-local character of weakly nonlinear waves; (ii) it is naturally simplified either to second-order Stokes waves, in the case of a flat bottom, or to the modified mild-slope equation, in the case of small-amplitude waves past a slowly varying bathymetry; (iii) it can be extended to treat obliquely incident waves, and study second-order refraction patterns; (iv) it can be used to formulate and study the second-order scattering matrix and nonlinear Bragg scattering over undulating topography.

Finally, the present theory can be extended to treat bichromatic and/or bidirectional wave–wave interactions in variable bathymetry regions, enabling the study of the statistical properties of second-order random seas in such regions, without imposing any mild-slope assumptions. However, special care should be taken in the calculation of the difference frequency potential, especially when the frequencies of the two interacting wave components come close to each other, or when the two wave

components are well separated in scale. In the first case, second-order bound (or locked) waves of high amplitude may appear as the particular solution at the second order, presenting deep penetration, Kim & Yue (1990). This could result in the excitation of second-order evanescent modes with large amplitudes and very slow rate of convergence of the corresponding second-order local-mode series. On the other hand, the interaction of a short wave riding on a long wave may not be described well by the conventional Stokes approach, due to possible modulation of the characteristics of the short waves by the presence of the long ones, Zhang, Hong & Yue (1993).

This work was partially supported by the Greek Secretariat for Research and Technology, in the framework of Joint Research and Technology Programme (2001–2002) between Greece and Poland. The authors are indebted to the referees for their constructive comments, and to Professor S. R. Massel, Institute of Oceanology, Polish Academy of Sciences, for his important comments and suggestions, which helped them to improve the presentation of this work.

Appendix A. Coefficients of the representations of the non-homogeneous second-order potentials in the two half-strips

The coefficients of the representation (4.6) of the second-order Stokes waves $p_{22}^{(1)}(x,z)$ and $e_{22}^{(1)}(x,z)$, bound to the linearized potential $\varphi_1^{(1)}(x,z)$ in the left half-strip $D^{(1)}$, are given by

$$\lambda_{0R} = -\mathrm{i}\frac{(3\mu^2 + (k_0^{(1)})^2)A_0A_R}{4\omega}, \tag{A 1a}$$

$$\lambda_0 = \frac{3\mathrm{i}\omega}{2}\frac{(\mu^2 - (k_0^{(1)})^2)A_0^2}{2k_0^{(1)}g\sinh(2k_0^{(1)}h_1) - 4\omega^2\cosh(2k_0^{(1)}h_1)}, \tag{A 1b}$$

$$\lambda_R = \frac{3\mathrm{i}\omega}{2}\frac{(\mu^2 - (k_0^{(1)})^2)A_R^2}{2k_0^{(1)}g\sinh(2k_0^{(1)}h_1) - 4\omega^2\cosh(2k_0^{(1)}h_1)}, \tag{A 1c}$$

$$\lambda_{0n} = -\frac{\mathrm{i}\omega}{g}\frac{(3\mu^2 + 2\mathrm{i}k_0^{(1)}k_n^{(1)} + \frac{1}{2}((k_n^{(1)})^2 - (k_0^{(1)})^2))A_0C_n^{(1)}\exp(-k_n^{(1)}a)}{(k_n^{(1)} + \mathrm{i}k_0^{(1)})\sin((k_n^{(1)} + \mathrm{i}k_0^{(1)})h_1) + \mu_2\cos((k_n^{(1)} + \mathrm{i}k_0^{(1)})h_1)},$$
$$n = 1, 2, 3, \ldots, \tag{A 1d}$$

$$\lambda_{Rn} = -\frac{\mathrm{i}\omega}{g}\frac{(3\mu^2 - 2\mathrm{i}k_0^{(1)}k_n^{(1)} + \frac{1}{2}((k_n^{(1)})^2 - (k_0^{(1)})^2))A_RC_n^{(1)}\exp(-k_n^{(1)}a)}{(k_n^{(1)} - \mathrm{i}k_0^{(1)})\sin((k_n^{(1)} - \mathrm{i}k_0^{(1)})h_1) + \mu_2\cos((k_n^{(1)} - \mathrm{i}k_0^{(1)})h_1)},$$
$$n = 1, 2, 3, \ldots, \tag{A 1e}$$

$$\lambda_{mn}^{(1)} = -\frac{\mathrm{i}\omega}{g}\frac{\left(\frac{3}{2}\mu^2 + \frac{1}{2}(k_n^{(1)})^2 + k_m^{(1)}k_n^{(1)}\right)C_m^{(1)}C_n^{(1)}\exp(-(k_m^{(3)} + k_n^{(3)})a)}{(k_m^{(1)} + k_n^{(1)})\sin((k_m^{(1)} + k_n^{(1)})h_1) + \mu_2\cos((k_m^{(1)} + k_n^{(1)})h_1)},$$
$$m, n = 1, 2, 3, \ldots. \tag{A 1f}$$

The coefficients of the representation (4.9) of the second-order Stokes waves $p_{22}^{(3)}(x,z)$ and $e_{22}^{(3)}(x,z)$, bound to the linearized potential $\varphi_1^{(3)}(x,z)$ in the right half-strip $D^{(3)}$ are given by

$$\lambda_T = \frac{3\mathrm{i}\omega}{2}\frac{(\mu^2 - (k_0^{(3)})^2)A_T^2}{2k_0^{(3)}g\sinh(2k_0^{(3)}h_3) - 4\omega^2\cosh(2k_0^{(3)}h_3)}, \tag{A 2a}$$

$$\lambda_{Tn} = -\frac{\mathrm{i}\omega}{g}\frac{(3\mu^2 - 2\mathrm{i}k_0^{(3)}k_n^{(3)} + \frac{1}{2}((k_n^{(3)})^2 - (k_0^{(3)})^2))A_T C_n^{(3)}\exp(k_n^{(3)}b)}{(k_n^{(3)} - \mathrm{i}k_0^{(3)})\sin((k_n^{(3)} - \mathrm{i}k_0^{(3)})h_3) + \mu_2\cos((k_n^{(3)} - \mathrm{i}k_0^{(3)})h_3)},$$
$$n = 1, 2, 3, \ldots, \tag{A 2b}$$

$$\lambda_{mn}^{(3)} = -\frac{\mathrm{i}\omega}{g}\frac{(\frac{3}{2}\mu^2 + \frac{1}{2}(k_n^{(3)})^2 + k_m^{(3)}k_n^{(3)})C_m^{(3)}C_n^{(3)}\exp((k_m^{(3)} + k_n^{(3)})b)}{(k_m^{(3)} + k_n^{(3)})\sin((k_m^{(3)} + k_n^{(3)})h_3) + \mu_2\cos((k_m^{(3)} + k_n^{(3)})h_3)},$$
$$m, n = 1, 2, 3, \ldots . \tag{A 2c}$$

The coefficients of the representation (4.12) of the known component $e_{20}^{(1)}(x, z)$ of the steady second-order wave potential $\varphi_{20}^{(1)}(x, z)$ in the left half-strip $D^{(1)}$, are given by

$$\tilde{\gamma}_{Rn} = -\frac{\mathrm{i}\omega}{2g}\frac{((k_n^{(1)})^2\bar{A}_R C_n^{(1)} - (k_0^{(1)})^2 A_0\bar{C}_n^{(1)})\exp(-k_n^{(1)}a)}{(k_n^{(1)} + \mathrm{i}k_0^{(1)})\sin((k_n^{(1)} + \mathrm{i}k_0^{(1)})h_1)}, \quad n = 1, 2, 3, \ldots, \tag{A 3a}$$

$$\gamma_{Rn} = \frac{\mathrm{i}\omega}{2g}\frac{(k_0^{(1)})^2(A_R\bar{C}_n^{(1)} - (k_n^{(1)})^2\bar{A}_0 C_n^{(1)})\exp(-k_n^{(1)}a)}{(k_n^{(1)} - \mathrm{i}k_0^{(1)})\sin((k_n^{(1)} - \mathrm{i}k_0^{(1)})h_1)}, \quad n = 1, 2, 3, \ldots, \tag{A 3b}$$

$$\gamma_{mn}^{(1)} = -\frac{\mathrm{i}\omega}{2g}\frac{(k_n^{(1)})^2\bar{C}_m^{(1)}C_n^{(1)}\exp(-(k_m^{(1)} + k_n^{(1)})a)}{(k_m^{(1)} + k_n^{(1)})\sin((k_m^{(1)} + k_n^{(1)})h_1)}, \quad m, n = 1, 2, 3, \ldots . \tag{A 3c}$$

Finally, the coefficients of the representation (4.15) of the known component $e_{20}^{(3)}(x, z)$ of the steady second-order wave potential $\varphi_{20}^{(3)}(x, z)$ in the right half-strip $D^{(3)}$, are given by

$$\tilde{\gamma}_{Tn} = -\frac{\mathrm{i}\omega}{2g}\frac{(k_0^{(3)})^2\bar{A}_T C_n^{(3)}\exp(k_n^{(3)}b)}{(k_n^{(3)} + \mathrm{i}k_0^{(3)})\sin((k_n^{(3)} + \mathrm{i}k_0^{(3)})h_3)}, \quad n = 1, 2, 3, \ldots, \tag{A 4a}$$

$$\gamma_{Tn} = \frac{\mathrm{i}\omega}{2g}\frac{(k_0^{(3)})^2 A_T\bar{C}_n^{(3)}\exp(k_n^{(3)}b)}{(k_n^{(3)} - \mathrm{i}k_0^{(3)})\sin((k_n^{(3)} - \mathrm{i}k_0^{(3)})h_3)}, \quad n = 1, 2, 3, \ldots, \tag{A 4b}$$

$$\gamma_{mn}^{(3)} = -\frac{\mathrm{i}\omega}{2g}\frac{(k_n^{(3)})^2\bar{C}_m^{(3)}C_n^{(3)}\exp((k_m^{(3)} + k_n^{(3)})b)}{(k_m^{(3)} + k_n^{(3)})\sin((k_m^{(3)} + k_n^{(3)})h_3)}, \quad m, n = 1, 2, 3, \ldots . \tag{A 4c}$$

Appendix B. Coefficients and forcing terms of the boundary conditions of the second-order coupled-mode systems

The coefficients $\chi_{n,r}$, $G_{n,r}$, $n = 0, 1, 2, \ldots$, $r = 2, 0$, appearing in the boundary conditions (7.8), are defined as follows:

$$\chi_{0,r}(a) = \begin{cases} \mathrm{i}\kappa_0^{(1)}, & r = 2 \\ 1, & r = 0 \end{cases}, \quad \chi_{0,r}(b) = \begin{cases} \mathrm{i}\kappa_0^{(3)}, & r = 2 \\ \xi, & r = 0 \end{cases}, \tag{B 1}$$

$$\chi_{n,r}(a) = \begin{cases} \kappa_n^{(1)}, & r = 2 \\ n\pi/h_1, & r = 0 \end{cases}, \quad \chi_{n,r}(b) = \begin{cases} \kappa_n^{(3)}, & r = 2 \\ n\pi/h_3, & r = 0 \end{cases}, \quad n = 1, 2, 3, \ldots . \tag{B 2}$$

The forcing terms $G_{n,2}$, $n = 0, 1, 2, \ldots$, appearing on the right-hand side of the boundary conditions (7.8) for the second-order wave problem ($r = 2$), are defined as follows:

$$G_{0,2}(a) = 2\mathrm{i}\kappa_0^{(1)}\Lambda_0^{(1)}\exp(\mathrm{i}\kappa_0^{(1)}a)$$
$$+\frac{1}{\|z_0^{(1)}\|^2}\int_{z=-h_1}^{z=0}(-\tilde{G}_2^{(12)}(z) + \chi_{0,2}(a)G_2^{(12)}(z))z_0^{(1)}(z)\,\mathrm{d}z, \quad n = 0, \tag{B 3}$$

$$G_{n,2}(a) = \frac{1}{\|z_n^{(1)}\|^2} \int_{z=-h_1}^{z=0} (-\tilde{G}_2^{(12)}(z) - \chi_{n,2}(a) G_2^{(12)}(z)) z_n^{(1)}(z)\,\mathrm{d}z, \quad n = 1, 2, \ldots, \tag{B 4}$$

$$G_{0,2}(b) = \frac{1}{\|z_0^{(3)}\|^2} \int_{z=-h_3}^{z=0} (\tilde{G}_2^{(23)}(z) - \chi_{0,2}(b) G_2^{(23)}(z)) z_0^{(3)}(z)\,\mathrm{d}z, \quad n = 0, \tag{B 5}$$

$$G_{n,2}(b) = \frac{1}{\|z_n^{(3)}\|^2} \int_{z=-h_3}^{z=0} (\tilde{G}_2^{(23)}(z) + \chi_{n,2}(b) G_2^{(23)}(z)) z_n^{(3)}(z)\,\mathrm{d}z, \quad n = 1, 2, \ldots, \tag{B 6}$$

where $\|\cdot\|$ denotes the usual L_2-norm. Note that the forcing term in the boundary condition of the propagating second-order mode $G_{0,2}(a)$, defined by equation (B 3), also carries the effects of the second-order free harmonic (with complex amplitude $A_0^{(1)}$), which is including in the generalized monochromatic incident wave system.

The forcing terms $G_{n,r}$, $n = 0, 1, 2, \ldots$, appearing on the right-hand side of the boundary conditions (7.8) for the steady second-order problem ($r = 0$), are defined as follows:

$$G_{0,0}(a) = \frac{1}{h_1} \int_{z=-h_1}^{z=0} G_0^{(12)}(z)\,\mathrm{d}z, \quad n = 0, \tag{B 7}$$

$$G_{n,0}(a) = \frac{1}{\|T_n^{(1)}\|^2} \int_{z=-h_1}^{z=0} (-\tilde{G}_0^{(12)}(z) - \chi_{n,2}(a) G_0^{(12)}(z)) T_n^{(1)}(z)\,\mathrm{d}z, \quad n = 1, 2, \ldots, \tag{B 8}$$

$$G_{0,0}(b) = v + \frac{1}{h_3} \int_{z=-h_3}^{z=0} \tilde{G}_0^{(23)}(z)\,\mathrm{d}z + \frac{\xi}{h_1} \int_{z=-h_1}^{z=0} \tilde{G}_0^{(12)}(z)\,\mathrm{d}z, \quad n = 0, \tag{B 9}$$

$$G_{n,0}(b) = \frac{1}{\|T_n^{(3)}\|^2} \int_{z=-h_3}^{z=0} (\tilde{G}_2^{(23)}(z) + \chi_{n,2}(b) G_2^{(23)}(z)) T_n^{(3)}(z)\,\mathrm{d}z, \quad n = 1, 2, \ldots. \tag{B 10}$$

Appendix C. Coefficients of the representations of the homogeneous second-order potentials in the two half-strips

The coefficients A_R, $A_n^{(1)}$, A_T, $A_n^{(3)}$ of the representation of the second-order wave potential ($r = 2$) in the two half-strips are expressed in terms of the solution of the corresponding second-order coupled-mode system by the relations

$$A_R = \left(f_{0,2}(a) - A_0 \exp(\mathrm{i}\kappa_0^{(1)} a) - \frac{1}{\|z_0^{(1)}\|^2} \int_{z=-h_1}^{z=0} G_2^{(12)}(z) z_0^{(1)}(z)\,\mathrm{d}z \right) \exp(\mathrm{i}\kappa_0^{(1)} a), \tag{C 1a}$$

$$A_n^{(1)} = f_{n,2}(a) - \frac{1}{\|z_n^{(1)}\|^2} \int_{z=-h_1}^{z=0} G_2^{(12)}(z) z_n^{(1)}(z)\,\mathrm{d}z, \quad n = 1, 2, 3, \ldots, \tag{C 1b}$$

$$A_T = \left(f_{0,2}(b) - \frac{1}{\|z_0^{(3)}\|^2} \int_{z=-h_3}^{z=0} G_2^{(23)}(z) z_0^{(3)}(z)\,\mathrm{d}z \right) \exp(-\mathrm{i}\kappa_0^{(1)} b), \tag{C 1c}$$

$$A_n^{(3)} = f_{n,2}(b) - \frac{1}{\|z_n^{(3)}\|^2} \int_{z=-h_3}^{z=0} G_2^{(23)}(z) z_n^{(3)}(z)\,\mathrm{d}z, \quad n = 1, 2, 3, \ldots, \tag{C 1d}$$

and the coefficients $\Gamma_n^{(1)}$, $\Gamma_n^{(3)}$, $n = 0, 1, 2, \ldots$, of the representation of the steady second-order potential ($r = 0$) by

$$\Gamma_0^{(1)} = \frac{\mathrm{d}f_{0,0}(a)}{\mathrm{d}x} - \frac{1}{h_1}\int_{z=-h_1}^{z=0} \tilde{G}_0^{(12)}(z)\,\mathrm{d}z, \tag{C 2a}$$

$$\Gamma_n^{(1)} = f_{n,0}(a) - \frac{1}{\|T_n^{(1)}\|^2}\int_{z=-h_1}^{z=0} G_0^{(12)}(z)T_n^{(1)}(z)\,\mathrm{d}z, \quad n = 1, 2, 3, \ldots, \tag{C 2b}$$

$$\Gamma_0^{(3)} = f_{0,0}(b) - \frac{1}{h_3}\int_{z=-h_3}^{z=0} G_0^{(23)}(z)\,\mathrm{d}z, \tag{C 2c}$$

$$\Gamma_n^{(3)} = f_{n,0}(b) - \frac{1}{\|T_n^{(3)}\|^2}\int_{z=-h_3}^{z=0} G_0^{(23)}(z)T_n^{(3)}(z)\,\mathrm{d}z, \quad n = 1, 2, 3, \ldots. \tag{C 2d}$$

REFERENCES

Athanassoulis, G. A. & Belibassakis, K. A. 1999 A consistent coupled-mode theory for the propagation of small-amplitude water waves over variable bathymetry regions. *J. Fluid Mech.* **389**, 275–301 (referred to herein as AB).

Athanassoulis, G. A., Belibassakis, K. A. & Gerostathis, Th. P. 2000 A coupled-mode theory for the diffraction of water waves by localized scatterers superimposed over a parallel-contour bathymetry. *Proc. 5th Intl Conf. on Mathematical and Numerical Models of Wave Propagation* (ed. A. Bermudez, D. Gomez, C. Hazard, P. Joly & J. Roberts), pp. 719–724. SIAM.

Beji, S. & Battjes, J. A. 1993 Experimental investigation of wave propagation over a bar. *Coastal Engng* **19**, 151–162.

Beji, S. & Nadaoka, K. 1997 A time-dependent nonlinear mid-slope equation for water waves. *Proc. R. Soc. Lond.* A **453**, 319–332.

Bendykowska, G. & Massel, S. 1984 Harmonic generation of waves due to submerged obsatcles. *Hydrotech. Trans., Polska Akademia Nauk Gdansk* **46**, 69–85.

Bendykowska, G. & Massel, S. 1988 On theory and experiments of mechanically generated waves. *Proc. 2nd Intl Symp. on Wave Research and Coastal Engng, Hannover*, pp. 401–413.

Chamberlain, P. G. & Porter, D. 1995 The modified mild-slope equation. *J. Fluid Mech.* **291**, 393–407.

Coddington, E. A. & Levinson, N. 1995 *Theory of Ordinary Differential Equations*, McGraw-Hill.

Dalzell, J. F. 1999 A note on finite depth second-order wave-wave interactions. *Appl. Ocean Res.* **21**, 105–111.

Debnath, L. 1994 *Nonlinear Water Waves*. Academic.

Dingemans, M. 1997 *Water Wave Propagation over Uneven Bottoms*. World Scientific.

Dommermuth, D. G. & Yue, D. K. D. 1987 Numerical simulations of nonlinear axisymmetric flows with a free surface. *J. Fluid Mech.* **178**, 195–219.

Drimer, N. & Agnon, Y. 1994 A hybrid boundary element method for second-order wave-body interaction. *Appl. Ocean Res.* **16**, 27–45.

Fenton, J. D. 1985 A fifth-order Stokes' theory for steady waves. *J. Waterway, Port, Coastal Ocean Engng, ASCE* **111**, 216–234.

Fontanet, P. 1961 Theorie de la generation de la houle cylindrique par un batteur plan. *La Houille Blanche* **16**, 174–197.

Goda, Y. 1997 Recurring evolution of water waves through nonresonant interactions. *Proc. 3rd Intl Symp. on Ocean Wave Measurement and Analysis Waves '97* (ed. H. Kim, S. H. Lee & S. J. Lee), pp. 1–23. ASCE; UIAM Publishers, Korea.

Grue, J. 1992 Nonlinear water waves at a submerged obstacle or bottom topography. *J. Fluid Mech.* **244**, 455–476.

Huang, C.-J. & Dong, C.-M. 1999 Wave deformation and vortex generation in water waves propagation over a submerged dike. *Coastal Engng* **37**, 123–148.

Huang, J. B. & Eatock Taylor, R. 1996 Semi-analytical solution for second-order wave diffraction by a truncated circular cylinder in monochromatic waves. *J. Fluid Mech.* **319**, 171–196.

HUDSPETH, R. T. & CHEN, M. C. 1979 Digital simulation of nonlinear random waves. *J. Waterway, Port, Coastal Ocean Engng*, *ASCE* **105**, 67–85.

HUDSPETH, R. T. & SULISZ, W. 1991 Stokes drift in two-dimensional wave flumes. *J. Fluid Mech.* **230**, 209–229.

HULSBERGEN, C. H. 1974 Origin, effect and suppression of secondary waves. *Proc. 14th Intl Conf. Coastal Engng*, pp. 392–411.

ISAACSON, M. 1982 Nonlinear wave effects on fixed and floating bodies. *J. Fluid Mech.* **120**, 267–281.

ISAACSON, M. & CHEUNG, K. F. 1991 Second-order wave diffraction around two-dimensional bodies by time-domain method. *Appl. Ocean Res.* **13**, 175–186.

ISAACSON, M. & CHEUNG, K. F. 1992 Time-domain second-order wave diffraction in three dimensions. *J. Waterway, Port, Coastal Ocean Engng*, *ASCE* **118**, 496–516.

JONSSON, I. G. & ARNEBORG, L. 1995 Energy properties of higher-order Stokes waves on a current. *Ocean Engng* **22**, 819–857.

KENNEDY, A. B. & FENTON, J. D. 1997 A fully non-linear computational method for wave propagation over topography. *Coastal Engng* **32**, 137–161.

KIM, M. H. & YUE, D. K.-P. 1990 The complete second-order diffraction solution for an axisymmetric body. Part 2. Bichromatic incident waves and body motions. *J. Fluid Mech.* **211**, 557–593.

KIOKA, W. & ISHIDA, H. 1993 Green's function approach to the weakly nonlinear interaction problem of two-dimensional structures of arbitrary cross-section. *Proc. JSCE* **461**, 59–65 (referred to herein as KI).

KIRBY, J. T. 1997 Nonlinear, disersive long waves in water of variable depth. In *Gravity Waves in Water of Finite Depth* (ed. J. N. Hunt), chap. 3. Computational Mechanics Publications.

KOJIMA, H., KIOKA, T. & YOSHIDA, A. 1990 Decomposition and interception of long waves by a submerged horizontal plate. *22nd Coastal Engng Conf.* (ed. B. Edge) vol. 2, chap. 92, 1228–1241 ASCE.

LI, W. & WILLIAMS, A. N. 1998 Second-order bichromatic wave loads on a semi-immersed horizontal rectangular cylinder. *Proc. 17th Intl Conf. on Offshore Mech. Arctic Engng OMAE98.* ASME.

LIGHTHILL, M. J. 1979 Waves and hydrodynamic loading. *Proc. Behaviour of Offshore Structures Conf. BOSS'79*, *London.*

LIU, P. L.-F. 1995 Model equations for wave propagation from deep to shallow water. In *Advances in Coastal and Ocean Engineering* (ed. P. L.-F. Liu). World Scientific.

LONGUET-HIGGINS, M. S. & COKELET, E. D. 1976 The deformation of steep surface waves on water. I: A numerical method of computation. *Proc. R. Soc. Lond.* A **350**, 1–25.

LOSADA, I. J., PATTERSON, M. D. & LOSADA, M. A. 1997 Harmonic generation past a submerged porous step. *Coastal Engng* **31**, 281–304.

MADSEN, P. A. & SORENSEN, O. R. 1992 A new form of Boussinesq equations with improved linear dispersion characteristics. 2. A slowly varying bathymetry. *Coastal Engng* **18**, 183–204.

MALENICA, S., EATOCK TAYLOR, R. & HUANG, J. B. 1999 Second-order wave diffraction by an array of vertical cylinders. *J. Fluid Mech.* **390**, 349–373.

MASSEL, S. 1983 Harmonic generation by waves propagating over a submerged step. *Coastal Engng* **7**, 357–380.

MASSEL, S. 1989 *Hydrodynamics of Coastal Zones.* Elsevier.

MASSEL, S. 1993 Extended refraction-diffraction equations for surface waves. *Coastal Engng* **19**, 97–126.

MEI, C. C. 1989 *The Applied Dynamics of Ocean Surface Waves.* World Scientific.

MOLIN, B. 1979 Second-order diffraction loads upon three-dimensional bodies. *Appl. Ocean Res.* **1**, 197–202.

MOUBAYED, W. I. & WILLIAMS, A. N. 1994 Second-order bichromatic waves produced by a generic plannar wavemaker in a two-dimensional flume. *J. Fluid Struct.* **8**, 73–92.

NADAOKA, K., BEJI, S. & NAKAGAWA, Y. 1997 A fully dispersive weakly nonlinear model for water waves. *Proc. R. Soc. Lond.* A **453**, 303–318.

NEWMAN, J. N. 1996 The second-order wave force on a vertical cylinder. *J. Fluid Mech.* **320**, 417–443.

NWOGU, O. 1993 Alternative form of Boussinesq equations for nearshore wave propagation. *J. Waterway, Port, Coastal Ocean Engng*, *ASCE* **119**, 618–638.

OHYAMA, T., JENG, D.-S. & HSU, J. R. C. 1995*a* Fourth-order theory for multiple-wave interaction. *Coastal Engng* **25**, 43–63.

Ohyama, T., Kioka, W. & Tada, A. 1995*b* Applicability of numerical models to nonlinear dispersive waves. *Coastal Engng* **24**, 297–313.

Ohyama, T. & Nadaoka, K. 1991 Development of a numerical wave tank for analysis of nonlinear and irregular wave field. *Fluid Dyn. Res.* **8**, 231–251.

Ohyama, T. & Nadaoka, K. 1994 Transformation of a nonlinear wave train passing over a submerged shelf without breaking. *Coastal Engng* **24**, 1–22 (referred to herein as ON).

Porter, D. & Chamberlain, P. G. 1997 Linear wave scattering by two-dimensional topography. In *Gravity Waves in Water of Finite Depth* (ed. J. N. Hunt), chap. 2. Computational Mechanics Publications.

Porter, D. & Staziker, D. J. 1995 Extension of the mild-slope equation. *J. Fluid Mech.* **300**, 367–382.

Rey, V., Belzons, M. & Guazzelli, E. 1992 Propagation of surface gravity waves over a rectangular submerged bar. *J. Fluid Mech.* **235**, 453–479.

Rhee, J. P. 1997 On the transmission of water waves over a shelf. *Appl. Ocean Res.* **19**, 161–169.

Schaeffer, H. 1996 Second-order wavemaker theory for irregular waves. *Ocean Engng* **23**, 47–88.

Stoker, J. J. 1957 *Water Waves.* Interscience.

Sulisz, W. 1993 Diffraction of second-order surface waves by semisubmerged horizontal rectangular cylinder. *J. Waterway, Port, Coastal Ocean Engng*, *ASCE* **119**, 160–171.

Sulisz, W. 1999 Nonlinear wave diffraction problem for a rectangular object. In *Nonlinear Water Wave Interaction* (ed. O. Mahrenholtz & M. Markiewicz). Advances in Fluid Mechanics, vol. 24, chap. 4. WIT Press.

Tang, Y. & Ouellet, Y. 1997 A new kind of nonlinear mild-slope equation for combined refraction-diffraction of multifrequency water waves. *Coastal Engng* **31**, 3–36.

Teng, B. & Kato, S. 1999 A method for second-order diffraction potential from an axisymmetric body. *Ocean Engng* **26**, 1359–1387.

Tsai, W. & Yue, D. K.-P. 1996 Computation of nonlinear free-surface flows. *Annu. Rev. Fluid Mech.* **28**, 249–278.

Vinje, T. & Brevig, P. 1981 Numerical simulation of breaking waves. *Adv. Water Resou.* **4**, 77–82.

Wang, P., Mirie, R. & Tulin, M. 1995 An efficient numerical tank for nonlinear water waves, based on the multi-subdomain approach with BEM. *Intl J. Numer. Meth. Fluids* **20**, 1315–1336.

Whitham, G. B. 1974 *Linear and Nonlinear Waves.* Wiley.

Wehausen, J. & Laitone, E. 1960 Surface waves. In *Encyclopedia of Physics*, vol. III, chap. 9. Springer.

Zhang, J., Hong, K. & Yue, D. 1993 Effects of wavelength ratio on wave modelling. *J. Fluid Mech.* **248**, 107–127.